

Clemson University

TigerPrints

All Theses

Theses

8-2024

Fault Detection and Location in Renewable-Fed Distribution Systems Using Low Voltage Sensors

Bushra Farhat
bfarhat@clemson.edu

Follow this and additional works at: https://open.clemson.edu/all_theses



Part of the [Power and Energy Commons](#)

Recommended Citation

Farhat, Bushra, "Fault Detection and Location in Renewable-Fed Distribution Systems Using Low Voltage Sensors" (2024). *All Theses*. 4343.

https://open.clemson.edu/all_theses/4343

This Thesis is brought to you for free and open access by the Theses at TigerPrints. It has been accepted for inclusion in All Theses by an authorized administrator of TigerPrints. For more information, please contact kokeefe@clemson.edu.

FAULT DETECTION AND LOCATION IN RENEWABLE-FED DISTRIBUTION SYSTEMS USING LOW VOLTAGE SENSORS

A Thesis
Presented to
the Graduate School of
Clemson University

In Partial Fulfillment
of the Requirements for the Degree
Master of Science
Electrical Engineering

by
Bushra Farhat
August 2024

Accepted by:
Dr. Sukumar Brahma, Committee Chair
Dr. Ramtin Hadidi
Dr. Christopher Edrington

Abstract

The penetration of Distributed Energy Resources (DERs) into the Electric Power System (EPS) is increasing. These (DERs) are mostly inverter-based resources (IBRs) that are integrated into (EPS) at the distribution level. Therefore, it has become necessary to leverage the integration of (IBRs) for both commercial and residential distribution systems through the deployment of Microgrid (MG). However, existing distribution systems that use fuses for sensing and isolating faults are not equipped to handle protection of microgrids where fault currents are fed from multiple sources and can flow downstream or upstream. Bulk of the protection schemes proposed in literature are heavily dependent on topology of distribution systems and connection status and location of IBRs. They also assume measurements at medium voltage (MV) buses which can be expensive.

To overcome these issues this thesis develops a source agnostic and topology agnostic protection scheme for microgrids using sensors at the low voltage (LV) side of all transformers feeding customers or connecting IBRs. The purpose is to have relatively inexpensive sensing across the microgrid. Synchronized voltages and current phasors are assumed to be transmitted by these sensors to a relay built in the central microgrid controller. A survey of existing commercial sensors is presented to justify this assumption.

Using this sensing mechanism, a novel scheme to detect a fault, identify the type of fault, and determine the faulted feeder-section is developed from fundamentals and extensively tested on the IEEE 13-bus feeder in grid connected and islanded modes with up to 100 % IBR penetration, clearly demonstrating the source and topology agnostic nature of the method. This scheme is intended to be a part of the Fault Location Isolation and Service Restoration (FLISR) module for microgrid.

Dedication

My family has my sincere dedication in my thesis. I was raised by parents who instilled in me the significance of education from an early age and taught me to respect it above all else.

Above all, I would express my gratitude to God for providing me with unwavering support and for sending me into the lives of those who encouraged and supported me along the way.

Acknowledgments

I express my gratitude to Dr. Sukumar Brahma, my advisor, for mentoring me throughout the process and providing me access to the tools I needed to complete this study. Besides that, I want to thank him for his time and patience in guiding me in the correct direction and for never ceasing to inspire me when things became tough. In addition, I want to express my gratitude to Dr. Christopher Edrington and Dr. Ramtin Hadidi for their time and work as members of my advisory committee and for their insightful feedback. Besides that, I would like to express my gratitude to Clemson University and its instructors for giving me the knowledge that made it easier for me to understand challenging technical ideas, that aided me in my research. Lastly, I express my gratitude to every lab member for their encouragement and assistance throughout my studies at Clemson University. Additionally, this endeavor would not have been possible without the generous support from Fulbright Program, who financed my Master's in Electrical Engineering at Clemson University.

Table of Contents

Title Page	i
Abstract	ii
Dedication	iii
Acknowledgments	iv
List of Tables	vii
List of Figures	viii
1 Introduction	1
1.1 Renewable-Fed Distribution System	1
1.2 Overview of MG Protection	2
1.3 Motivation for FLISR scheme using LV Sensors	4
1.4 Requirements and Available LV (Sensors/Devices)	5
1.5 Summary of Chapter 1	10
2 Concept of Proposed Scheme	11
2.1 Calculation of MV Voltages	11
2.2 Calculation of Line Currents	13
2.3 Calculation of KCL at a Bus	15
2.4 Application of KCL in Steady State	16
2.5 Application of KCL for a Faulted Feeder	18
2.6 Summary of Chapter 2	21
3 Methodology	22
3.1 General Methodology	22
3.2 Fault Detection	24
3.3 Fault Identification	25
3.4 Faulted Feeder Location	27
3.5 Summary of Chapter 3	29
4 Relay Design and Algorithm	31
4.1 Important Parameters of Relay Design	31
4.2 Overview of Algorithm for Fault Detection and Identification	33
4.3 Overview of Algorithm for Faulted Feeder Location	35
4.4 Summary of Chapter 4	38
5 Test System	39
5.1 Distribution Line Model	39

5.2	Connection of Inverter Based Resources (IBRs)	41
5.3	Low-Voltage (120 V) Loads	42
5.4	Computation of KCL expressions for the Test System	46
5.5	Summary of Chapter 5	46
6	Simulation	47
6.1	Simulation Software	47
6.2	Fault Resistance	48
6.3	Steady State Simulation	48
6.4	Fault Testing and Simulation	49
6.5	Dynamic Scenarios Simulation	52
6.6	Summary of Chapter 6	53
7	Conclusions and Discussion	55
7.1	Further Research	56
Appendices		57
A	KCL Expressions for the Test System	58
Bibliography		60

List of Tables

5.1	Load Transformers Data	44
6.1	Results for Steady-State Simulation	48
6.2	Fault Scenarios for Testing	49
6.3	Results for Load Switching	52
6.4	Results for Capacitor Switching	52
6.5	Results for Transformer Inrush	53

List of Figures

2.1	Single-Bus Distribution System	12
2.2	Two-Bus Distribution System	14
2.3	Two-Bus Distribution System with IBR	15
2.4	Current Flows for the System shown in Figure 2.3 During Steady-State	17
2.5	Current Flows for the System shown in Figure 2.3 During Fault	19
3.1	General Overview of FLISR Scheme	23
3.2	Areas of IEEE 13 Bus System	28
4.1	Algorithm for Fault Detection and Identification	34
4.2	Algorithm for Location of Faulted Feeder	37
5.1	IEEE 13 Bus System	40
5.2	Three-phase Line Segment Model	41
5.3	IBRs in IEEE 13 Bus System	42
5.4	Final Test System	45

Chapter 1

Introduction

Recently, the penetration of inverter-based resources (IBRs) in the electric distribution systems is significantly increasing [1]. Therefore, it has become necessary to leverage the integration of IBRs at secondary distribution voltages properly to avoid any compromises in system security. That is why the deployment of Microgrids (MG) has become crucial for a distribution system that maintains the resiliency of any power system by utilizing its two modes of operation - Grid-Connected Mode and Islanded mode. So when there is an outage, a MG can seamlessly switch to Islanded mode in which typically a grid-forming inverter assumes the role of main grid [2]. However, as compared to conventional bulk power system, which has well-established methods and protection schemes available for detection and determination of fault location, fault-type identification and de-energization of the faulted equipment in a selective manner, microgrids have brought unique challenges when it comes to protection scheme development [3]. Therefore, in this report, a *Fault Detection, Identification and Location* scheme is developed for MV systems penetrated by IBRs using *LV Sensors*.

1.1 Renewable-Fed Distribution System

Recently, AC microgrids have been increasingly deployed at secondary distribution systems. The voltage for commercial and residential applications is (480V) and (120V/240V) for distribution networks in the United States. It is said that future microgrids will emerge from real-life distribution feeders rather than custom-built on a specific topology [2]. This has led to a more decentralized and

distributed system than ever before [4]. For example, several rooftop photovoltaic (PV) panels are connected to the main grid at a residential distribution voltage of 120 V. In this context, the system interconnection of IBRs to the main grid at a distribution scale of voltage (480V) or (120V/240V) is regarded as a ‘Renewable-Fed Distribution System’ in this report.

1.2 Overview of MG Protection

This section overviews MG protection based on available literature and survey papers [3]. It also briefly describes the challenges of MG protection and existing protection schemes.

1.2.1 Challenges of Microgrid Protection

The major challenges of MG protection result from variable fault current levels in two modes of operation of MG, bidirectional power flow in feeders, and low fault current contribution from IBRs. Besides, renewable-fed systems have low system inertia and sensitive loads, which require fast operation [3]. Due to these factors, the following major challenges are encountered while developing a protection scheme for MG:

1.2.1.1 Simulation Challenge for IBR short circuit (SC) analysis

The fault characteristic of IBRs is relatively different compared to traditional synchronous generation sources. As a result, conventional phasor domain analysis programs based on the Thevenin equivalent circuit can produce incorrect results [1]. That is why a comprehensive Electromagnetic Transients (EMT) program based on time-domain analysis needs to be used to produce practical results. Therefore, the capabilities of software tools should be analyzed before modeling of IBRs for the proposed protection scheme.

1.2.1.2 Maintaining Dependability For Grid- Interconnected and Islanded Mode

Depending on the mode of operation, the available fault current (AFC) level could be different at the Point of Common Coupling (PCC). Besides that, the fault current magnitude of IBRs is limited to only **1.2-1.5 per unit** compared to conventional source connected to the distribution feeder. This does not only lead to the misoperation of overcurrent protective devices but renders

a typical fuse-recloser scheme infeasible due to bi-directional power in renewable-fed distribution systems [5].

1.2.1.3 Conventional Protection Schemes mis-operation

Because of the challenges imposed by MG, conventional protection and control schemes may have the possibility of misoperating in proper detection, location and isolation of fault. For instance, applying under-voltage protection as a primary choice is not the best fit because both IBRs and distributed loads are close, as feeder distances are smaller in distribution systems. This can lead to misidentification of faulted feeder [4]. Similarly, Distance Protection, which is fairly efficient for transmission systems, might misoperate in distribution systems due to the problem of over-reach and under-reach because distribution lines have several branches [1].

1.2.1.4 Topology And Generation Changes

There is a lack of general primary and secondary protection schemes for every size and topology of MG. It is possible that a protection scheme valid for a specific MG may not be completely implemented for another MG due to limitations in cost, system size, and infrastructure. Recently, a paper on [2] addresses this problem of scalable protection schemes independent of the number, location and placement of sources.

1.2.2 Available Protection Schemes

Due to the challenges posed by MGs, unique and customized protection and control schemes have been developed to facilitate the growth of IBR penetrated systems. After conducting a thorough literature review of existing and available protection schemes for MG, these protection schemes are found to be distinguished, which are described as follows:

1.2.2.1 Adaptive Protection

As implied by the name, the adaptive method of protection includes modifying the protective device settings and protection settings group in real-time as changes occur in the system's operating conditions [6]. Though adequate, adaptive protection significantly increases the cost of the protection scheme.

1.2.2.2 Directional Interlocking Scheme

Directional Interlocking Scheme, also known as Zone Selective Interlocking Scheme (ZSI), includes the direction of current flowing into a protection zone. This system information is relayed in real-time to a controller to issue a tripping signal to an appropriate protective device. However, this scheme can significantly increase the system's cost due to the implementation of directional relays in each feeder of the distribution network [1].

1.2.2.3 Centralized Fault Detection Scheme

The centralized fault detection scheme works by installing several sensing devices throughout the power system. This scheme is advantageous over other schemes because it integrates fault location isolation and service restoration (FLISR) through a single controller, which enhances fault management. This scheme can be implemented in two ways.

In the first method, when a fault occurs on the system, it is detected and cleared by local protection and 'breaker status' is reported to the central controller. According to [7], the central controller could either be software based on an algorithm or an upper protection relay in the main substation.

In the second method, when a fault occurs, the central controller receives real-time measurements directly from remote Intelligent Electronic Devices (IEDs). Then, it utilizes this information to determine the location of the fault. Lastly, the controller transfers the tripping signals to the appropriate fault-clearing device to completely isolate the fault from the system. Now, with the advancement in distribution automation and the recent development of IEDs at the distribution system level, the second method is preferred over the previous one as it avoids the high cost of installing separate protective relays on each distribution system feeder. Instead, sensors and IEDs are already available at the distribution scale for monitoring, and measurements can be utilized to transfer relevant information to the system. Therefore, this report's proposed FLISR protection scheme for renewable-fed distribution is also based on this method.

1.3 Motivation for FLISR scheme using LV Sensors

There are three major motivators in pursuing this study, which are described as follows:

First, any protection scheme must be designed considering all the challenges imposed by

MG protection discussed in the previous section. Therefore, the proposed protection scheme for the fault detection, identification and location of renewable-fed distribution systems must also withstand the challenges (MG) poses. These challenges include modeling and simulation for IBR short circuit analysis and dependability for grid-connected and islanded modes of operation.

As mentioned, there is a lack of general and topology-agnostic protection schemes for (MG). This makes the scheme costly and infeasible for widespread implementation in distribution systems. Therefore, the proposed protection scheme must also apply to other systems regardless of their topology, number of buses, placement of sources and infrastructure.

Most importantly, the published literature on MG protection does not show any papers on any (FLISR) scheme for (MV) systems using (LV) sensors. That is, it only shows the concept of Centralized Fault Detection, but the implementation of (FLISR) through low-voltage, distributed sensors has yet to be present, which serves as a motivation for the development of the proposed protection scheme.

1.4 Requirements and Available LV (Sensors/Devices)

As discussed previously, leveraging (IED) features of local sensing of current and voltage along with a central controller is a novel scheme of MG protection. With that being said, the following questions are put forward for the practical implementation of FLISR using LV sensors:

- What existing sensors/ IEDS are commercially available in the market that provide local sensing of current and voltage that can be used for MG protection, particularly renewable-fed distribution systems?
- Is it possible to link the available IEDs to a central controller for optimal performance?
- What are the significant requirements of those IEDs for implementing the FLISR scheme?

The above questions are addressed in the following two subsections.

1.4.1 Main Requirements of (IEDs)

For the successful implementation of the proposed protection scheme, which is the FLISR of MV systems in renewable-fed distribution systems, a list of essential requirements from LV sen-

sors/devices is made. Any LV Sensor/Device, either explained in this section or currently being developed, can be utilized for this scheme if it has the following features:

1.4.1.1 Telemetry and Remote communication

LV Sensors should be capable of remotely transmitting information to a central system in real-time. It should work seamlessly on substation automation protocols, such as Distributed Network Protocol 3 (DNP3), to relay information wirelessly to the central system. The sensor/device must be able to transmit **8 phasors per cycle** to the central system so as not to overburden the communication network of the central controller. This is further explained in Chapter 6, relay design.

1.4.1.2 Time-scale of Synchronized Measurements

LV sensors must be capable of measuring at least three-phase voltages and currents with accurate synchronization capability and transmitting this information to a central system in real time. Fault management like FLISR is possible only when measurements are received in protection time of operation, around *1 - 2 cycles*. Besides that, all measurements obtained by the central controller should be time-synchronized.

1.4.1.3 Distribution Voltage

The rated voltage of LV Sensors and Devices must be suitable for distribution systems (120/240V) for residential and (480V) for commercial applications in the United States.

Based on an above-mentioned list of requirements, the following LV sensors and devices come closest to meeting most or all of the expectations.

1.4.2 Available Low-Voltage Sensors

This section gives an overview of existing LV sensors and devices discussed in the literature and commercially available from prominent industry manufacturers for distribution systems. The main benefit of both LV sensors and devices is their cheaper cost and smaller size, which makes them ideal for wide-scale implementation of renewable-fed distribution systems. This section discusses different designs of existing voltage and current sensors available at residential service at (120V/240V). This is based upon the technical guide of commercially available sensors by manufacturers cited in

[8], [9] and [10]. Different designs of low-voltage sensors are classified majorly into the following types:

1.4.2.1 Voltage Divider

As the name implies, a voltage divider consists of a linear circuit that can produce an output voltage proportional to the fraction of its input voltage. A voltage divider circuit can be further divided into resistive and capacitive divider circuits depending on the element type used to divide the output voltage.

1.4.2.2 Hall Effect Voltage Sensor

Voltage sensors based on Hall Effect technology are called Hall Effect voltage sensors.

1.4.2.3 Electronic Voltage Sensor

Compared to the Hall effect sensors, electronic sensors do not comprise any Hall effect probes for voltage measurement. As a result, electrical insulation is provided between primary and secondary circuits. [11].

Similarly, designs of LV Currents sensors is classified majorly into the following:

1.4.2.4 Hall Effect Current Sensor

A voltage produced by a Hall effect sensor is proportional to the magnetic field that passes through it [11]. As a result, external magnetic fields can affect the sensor output.

1.4.2.5 Electronic Current Transformer (CT)

These current sensors work on the principle of a CT in stepping down the current for a secondary circuit proportional to the current in the primary circuit. However, instead of a magnetic circuit, they are based entirely on electronic technology[11].

1.4.2.6 Rogowski coil

Rogowski coil is an air core CT formed by winding a coil on a non-magnetic core. A magnetic field is created when a conductor experiences an alternating or pulsed current. This mag-

netic field interacts with the nearby Rogowski coil to produce an induced voltage in the coil that is proportionate to the rate at which the measure current changes.

1.4.2.7 Final Remarks on Available Sensors

The explanation of the different approaches of sensor designs could be used to develop, implement, and even modify their features as IEDs for effective fault management in renewable-fed distribution systems. As of today, the commercially available sensors from electric manufacturers meet only two out of three requirements. Excluding wireless data transmission and suitable distribution voltages, these sensors are still majorly utilized for monitoring and metering purposes rather than fault management, which requires data transmission in the protection time of scale mentioned earlier. However, the current trends in sensing technologies suggest the proliferation of wireless sensors across distribution systems [12], [13], that would be capable of not only measuring power quantities in real-time but also providing time-synchronized information to a central system [14] in protection time of operation. For instance, sensors shown in [14] have wireless interface for energy and voltage monitoring for extensive applications, including fault management. Besides that, the survey on smart 'stick on' sensors in [15] and [16] lays out the requirements for universal sensors and IEDs for more efficient asset monitoring in power systems.

1.4.3 Available LV Devices

Compared to sensors, devices combine voltage and current sensors, also known as '**combi-sensor**', which complements their functionality. This section gives an overview of the available devices for distribution systems that meet all or most of the essential requirements of the proposed scheme.

1.4.3.1 Fault Passage Indicators

Remote Fault Indicators (RFIs) / Fault Circuit Indicators (FCIs) are the different terms used for Fault Passage Indicators (FPIs). FPI is a combi sensor installed on each phase of a distribution feeder [7]. Until the last decade, FPIs were mainly used for outage management. Similar and advanced FPIs have recently been built specifically for fault management in distribution systems [17]. The FPIs from [7] can measure and provide information about three-phase current and voltages

to an upper central system in a synchronized manner. Based on that, a central system is capable of not only doing asset monitoring but also remote controlling for the isolation of fault. The rated voltage of FPIs starts from (480V) which is suitable for commercial distribution systems.

1.4.3.2 Micro Phasor Measurement Unit (μ PMU)

Due to its high cost and widespread use in distribution networks, PMU has, up until now, mainly been used in transmission networks [18]. Therefore, μ PMU is a measurement device that provides the synchronized voltage and current phasors, primarily for distribution circuits with minor angle differences and several nodes [19]. That is why it is also called distribution level PMU [18]. Micro PMUs can provide real-time synchrophasor data up to 120 frames per second [20]. μ PMU can be directly connected to low-voltage distribution networks worldwide up till 690 V [21]. Compared to its installation on medium-voltage distribution lines, the induced errors of instrument transformers/transducers can be avoided entirely, which is critical for μ PMUs in providing accurate voltage and current synchro-phasors to the central system [19]. This further encourages the installment of μ PMU on secondary distribution circuits, rated at (120V/240V) for residential and (480 V) for commercial applications in the United States, which are selected for the proposed protection scheme.

1.4.3.3 Smart Meters and Power Analyzers

Smart Meters (SMs) are devices used for monitoring and outage management in emerging distribution systems. According to [22], SMs have come a long way from offline automated meter reading (AMR) to time-based synchronized measurements of power quantities and data processing [22]. Similarly, the advanced SMs incorporate the transmission/receiving of data remotely between the meter and central system. Besides that, a power analyzer is another device that can detect power quality problems and provide real-time readings and event alerts to the central system [23].

1.4.3.4 Final Remarks on Available Devices

Like sensors, smart meters and power analyzers transmit data at a time scale suitable only for energy measurement and monitoring instead of the required operation time for protection. This is an existing challenge for its implementation in fault management [22]. However, there has been a change in progress in the utilization of distributed measurements in fault management, including SMs. For instance, according to the final report by Quanta Technology available at

[24] , the successful actualization of different applications of synchronized measurements across the distribution systems will reduce the time of data communication significantly and will enable higher speed of fault detection and isolation than seen before. Nonetheless, the devices like FPI and μ PMU have all the features and capabilities to fulfil all the requirements mentioned in section 1.4, including the mandatory protection time of operation for fault management.

1.5 Summary of Chapter 1

In summary, microgrids support the efficient integration of IBRs in distribution systems. Besides the benefits of MG, there are associated challenges when developing protection schemes for MG because of the introduction of variable fault levels and the bi-directional flow of current. Conventional protection schemes are limited in locating and identifying faults in MG selectively; therefore, customized logic and protection schemes are described, including a centralized fault detection scheme for (FLISR) management. The idea of implementation of the (FLISR) scheme for (MV) systems using (LV) distributed sensors is a novel protection scheme. Finally, the main features of LV sensors/devices required for successfully implementing the proposed scheme in this report are highlighted. Besides that, a comparison of already available sensors/devices is done to fulfill the requirements. FPI from [7] and μ PMUs meet all the requirements for the proposed protection scheme, including remote communication, protection time-scale of synchronized measurements, and rating for distribution systems, making either of them an ideal choice for the proposed FLISR scheme.

Chapter 2

Concept of Proposed Scheme

This chapter explains the basic concept of the proposed protection scheme. It is essential to calculate the respective quantities on the MV side for the fault detection, identification and location of MV systems using LV sensors. Therefore, this chapter includes the rationale and expressions for the computation of specific MV quantities required for FLISR implementation. In addition, the fundamental concept of using computed parameters to identify faulty feeders is also explained. Based on this, the following chapter uses the ideas covered in this chapter to outline the methodology of the proposed protection scheme.

2.1 Calculation of MV Voltages

A three-phase diagram of a single-bus distribution system is shown in Figure 2.1. The source is connected through a distribution transformer rated at 115kV/4.16kV to the system. Here, the connection of the main transformer is selected as $(\Delta - Y_g)$ which is typical for a distribution network as they are unbalanced in nature. Then, a three-phase unbalanced load is connected to Bus 1 by $(Y_g - Y_g)$ three-phase transformer rated at 4.16kV/0.208kV. This means that each phase of the load is rated at 120 V which is suitable for the placement of LV sensors described in Chapter 1. For the ease of calculation, $(Y_g - Y_g)$ transformer connection is chosen as it has a phase shift of 0° . Let's call the load transformer connected to Bus 1 as 'Transformer 1' having an impedance of 0.03j per unit.

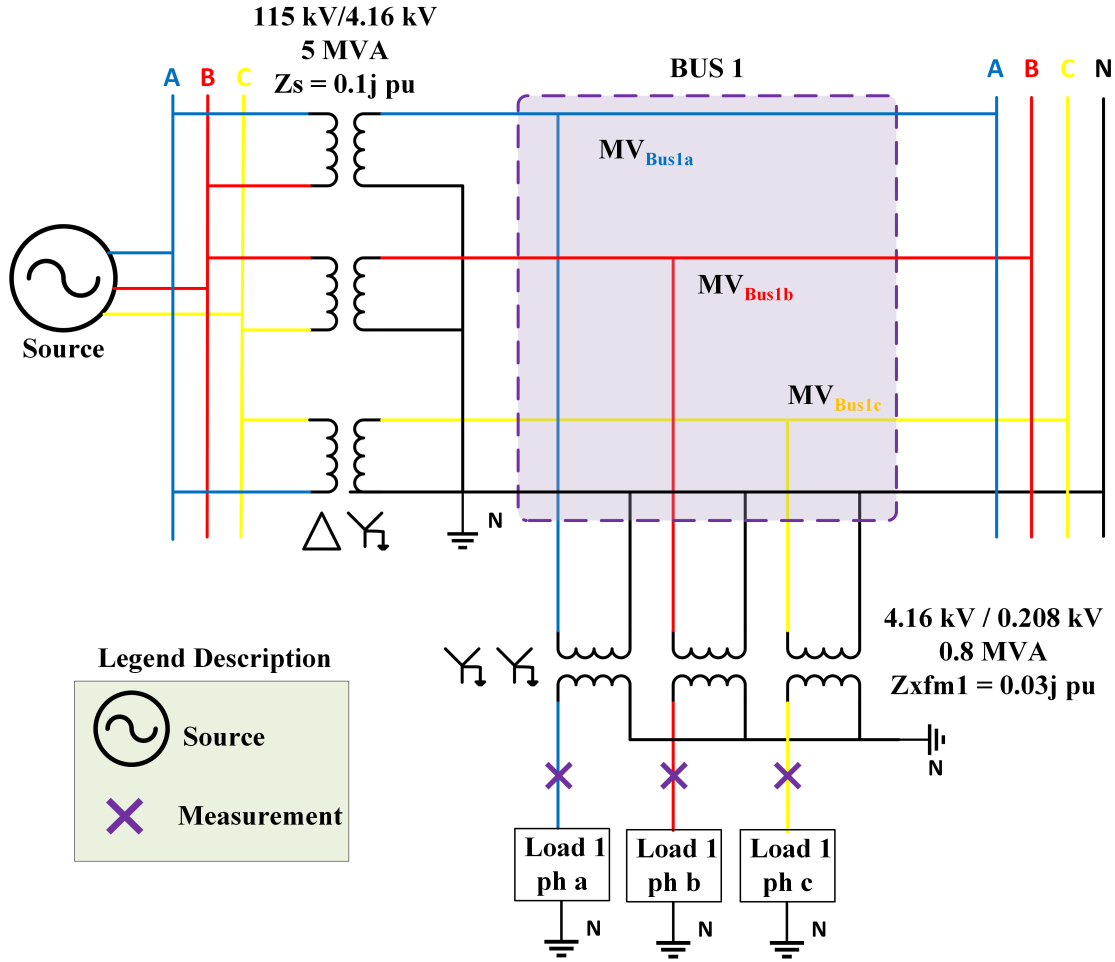


Figure 2.1: Single-Bus Distribution System

Based on the requirements for centralized fault detection explained in the previous chapter, we can deduce that the central controller (CC) is consecutively gathering and analyzing time-synchronized phasor quantities from the LV side of each phase of Transformer 1, that is, $120 V_{rated}$ for each phase. As analysis is required on the MV side, the three-phase voltage phasors must be reflected on the primary side of Transformer 1, $2401.8 V_{rated}$ for each phase. The conversion to three-phase primary (MV) phasors from three-phase secondary (LV) phasors of Transformer 1 can be done using Equation 2.1:

$$MV_{Bus1} = (LV_{Bus1} \times T_{xfm1}) + (Z_{xfm1})(I_{Load1} \times 1/T_{xfm1}) \quad (2.1)$$

where,

MV_{Bus1} is the (3x1) matrix of three-phase, medium-voltage phasors calculated at Bus 1 (2401.8 V_{rated} for each phase).

LV_{Bus1} is the (3x1) matrix of three-phase, low-voltage phasors received from LV side of Transformer 1 that is, (120 V_{rated} for each phase).

I_{Load1} is the (3x1) matrix of three-phase, load-current phasors obtained from LV side of Transformer 1

T_{xfm1} is the turns-ratio of Transformer 1. It is $\frac{2401V}{120V} = 20$ for the given case.

Z_{xfm1} is the impedance of Transformer 1 in per unit which is 0.03j pu for the given case.

Turns ratio and impedance of the transformer are constant parameters that can be easily obtained from system database. In this way, the central controller can calculate the MV Bus voltages for all the load buses in the system.

2.2 Calculation of Line Currents

Consider addition of another three-phase load to the previous system as shown in Figure 2.2. The additional load is connected at Bus 2 through a three phase transformer rated at 4.16kV/0.208kV having an impedance of 0.025j per unit. The three-phase medium-voltage phasors at Bus 2 can be calculated in the same manner by using Equation 2.1.

Once, three-phase medium-voltage phasors are calculated both for Bus 1 and Bus 2, the three-phase current phasors representing the line currents flowing from Bus 1 to Bus 2 can be calculated using Equation 2.2:

$$I_{Line12} = inverse(Z_{Line12}) \times (MV_{Bus1} - MV_{Bus2}) \quad (2.2)$$

where,

I_{Line12} represents the (3x1) matrix of three-phase current phasors calculated for the line between Bus 1 and Bus 2.

Z_{Line12} represents the (3x3) phase impedance matrix of the distribution line/feeder between Bus 1 and Bus 2.

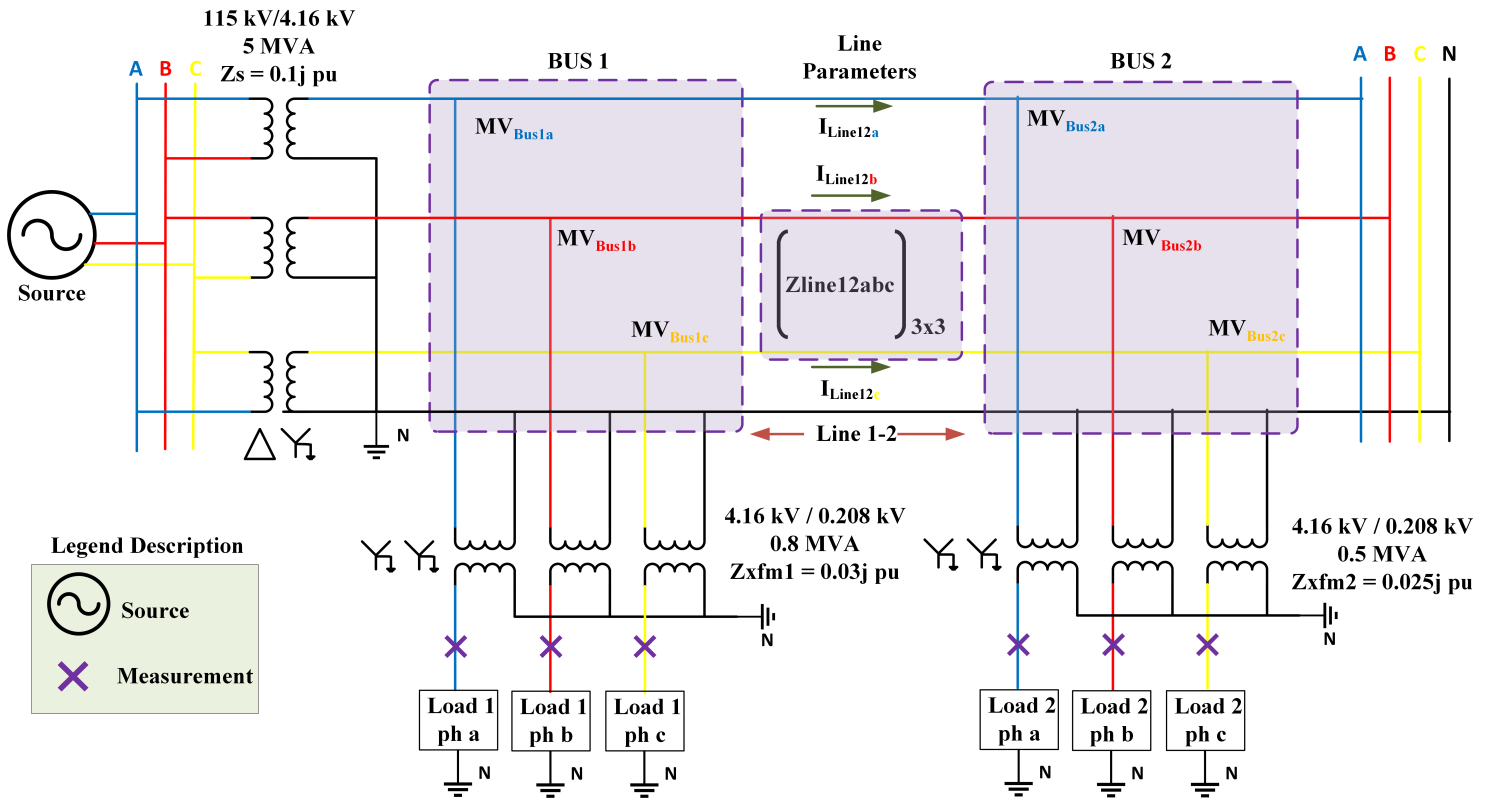


Figure 2.2: Two-Bus Distribution System

MV_{Bus1} represents the (3×1) matrix of three-phase, medium-voltage phasors calculated for Bus 1.

MV_{Bus2} represents the (3×1) matrix of three-phase, medium-voltage phasors calculated for Bus 2.

The exact parameters of a line/feeder, that is the phase impedance matrix, can be easily obtained from electric utility which is governing the distribution system. If exact parameters could not be obtained, system information including conductor or cable data can be utilized to calculate these parameters. More information about the line parameters can be found in Chapter 5.

Nonetheless, from this method the three-phase current phasors can be calculated for any line/feeder using Equation 2.2

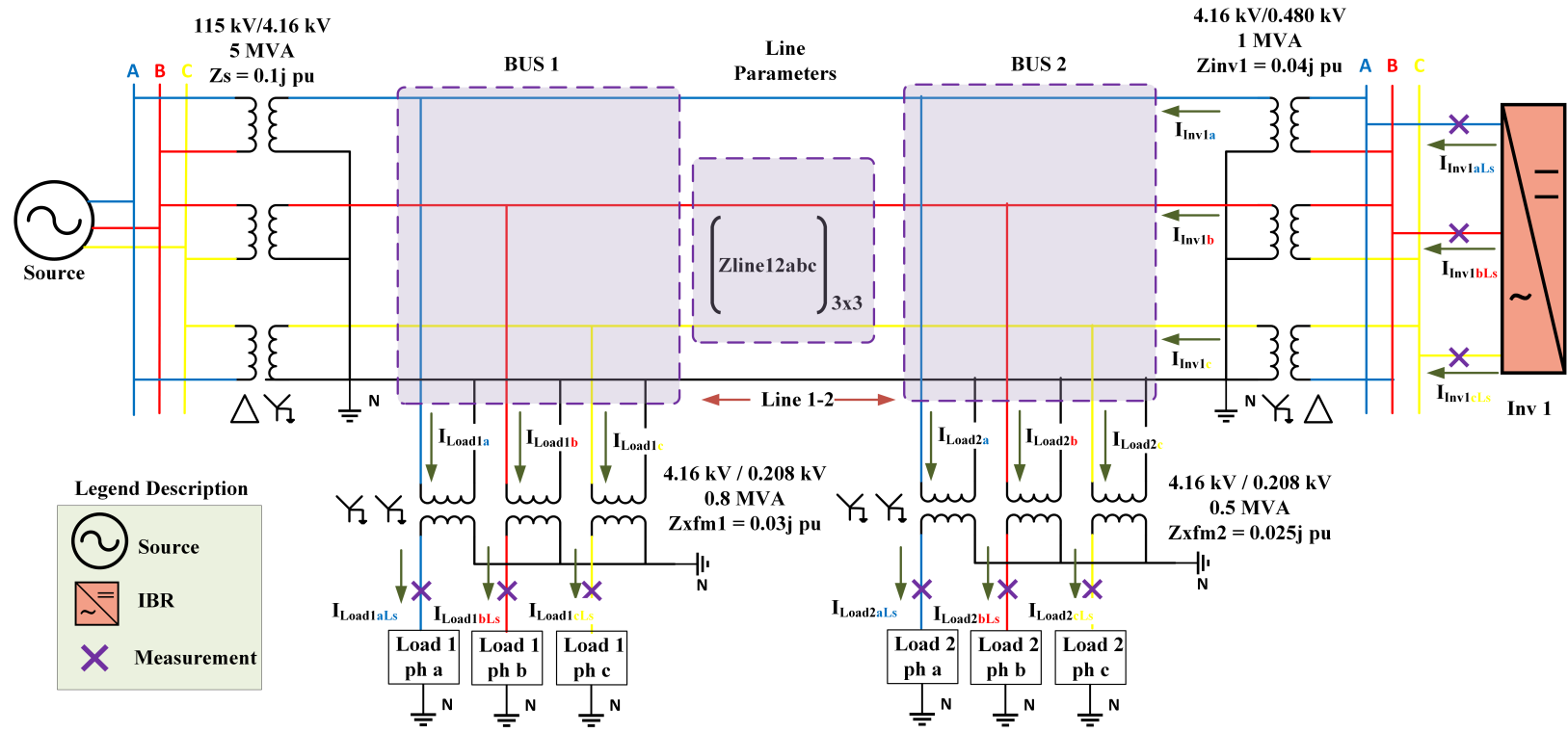


Figure 2.3: Two-Bus Distribution System with IBR

2.3 Calculation of KCL at a Bus

Consider an IBR that is connected at Bus 2 to the previous system as shown in Figure 2.3. The IBR is connected through a ($Y_g - \Delta$) three-phase transformer rated at (4.16kV/0.480kV). LV sensors are placed at each phase of the IBR rated at 277V. The ($Y_g - \Delta$) transformer connection for the IBR is selected specifically as grid-following inverters produce negligible negative and zero sequence currents. Therefore, by having (Y_g) connection on primary, system grounding is completed and the transformer acts as a separate derived source of zero sequence current for unbalanced faults in the system [3].

Nonetheless, the central controller consecutively gathers and analyses time-synchronized, three-phase current phasors from secondary side of load transformers ($120 V_{rated}$ for each phase) as well as for grid-following inverters ($277 V_{rated}$ for each phase). As the turns-ratio of each transformer is known, controller can calculate the three-phase current phasors on the medium-voltage, primary side of each transformer that is, $2401.8 V_{rated}$ for each phase. Therefore, the three-phase current

phasors supplied by the IBR can be calculated from Equation 2.3.

$$I_{inv1} = (I_{inv1Ls}) \div (T_{inv1}) \quad (2.3)$$

where,

I_{inv1} represents the (3x1) matrix of three-phase current phasors calculated to show the currents supplied to Bus 2 by the inverter 1 (2401.8 V_{rated} for each phase).

I_{inv1Ls} represents the (3x1) matrix of three-phase current phasors obtained from LV side of connected transformer (277 V_{rated} for each phase).

T_{inv1} is the turns-ratio of IBR connected Transformer. It is $\frac{2401V}{277V} = 8.7$ for the given case.

As seen in Figure 2.3, inverter is connected through a ($Y_g - \Delta$) transformer, so, there must be a 30° phase shift for conversion of three-phase currents from LV to MV side. This phase shift needs to be accounted as well for accurate reflection of MV phasors from LV. Similarly, three phase primary currents consumed by the unbalanced load can be calculated from 2.4.

$$I_{Load2} = (I_{Load2Ls}) \div (T_{xfm2}) \quad (2.4)$$

where,

I_{Load2} represents the (3x1) matrix of three-phase current phasors calculated on the primary side of Transformer 2 (2401 V_{rated} for each phase).

$I_{Load2Ls}$ represents the (3x1) matrix of three-phase current phasors obtained from the secondary side of transformer 2 (120 V_{rated} for each phase).

T_{xfm2} is the turns-ratio of Transformer 2 which is $\frac{2401V}{120V} = 20$ for the given case.

2.4 Application of KCL in Steady State

Nonetheless, based on the phasor quantities obtained from the LV side of connected loads and IBRs, the central controller can calculate three-phase line current phasors representing current flows from Bus 1 to Bus 2 as well as three-phase current phasors consumed/supplied by all loads and connected inverters on MV side respectively. Now that all the time-synchronized, three-phase current phasors at Bus 2 are calculated, representing all incoming and outgoing currents to/from

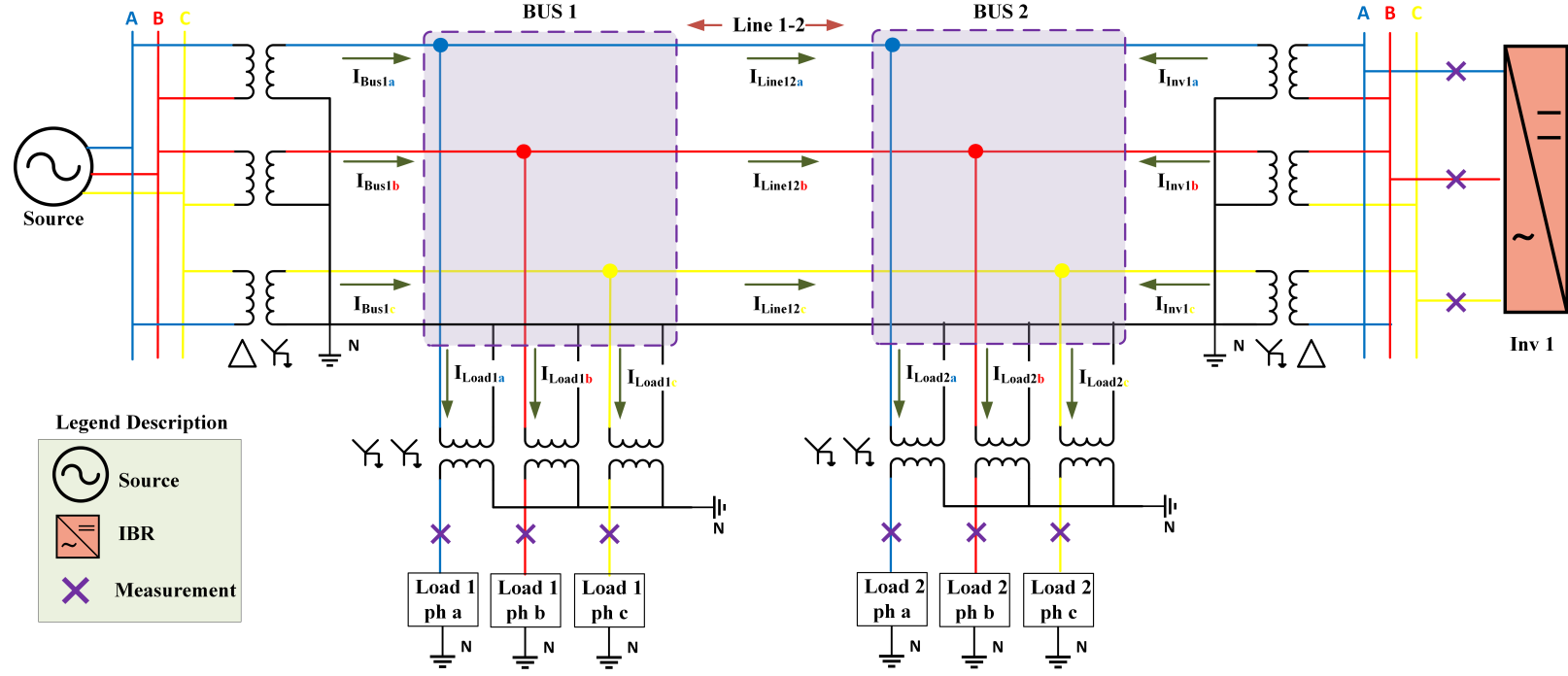


Figure 2.4: Current Flows for the System shown in Figure 2.3 During Steady-State

Bus 2, Kirchoff's Current Law (KCL) can be easily computed at Bus 2. See Figure 2.4 for all the current inflows and outflows for the previous system. Therefore, KCL at Bus 2 can be computed using Equation 2.5.

$$KCL_{Bus2} = I_{Line12} - I_{Load2} + I_{inv1} \quad (2.5)$$

where,

KCL_{Bus2} represents the (3x1) matrix of the KCL computed at Bus 2.

I_{Line12} represents the (3x1) matrix of three-phase current phasors calculated previously.

I_{Load2} represents the (3x1) matrix of three-phase current phasors calculated previously.

I_{inv1} represents the (3x1) matrix of three-phase current phasors calculated previously.

Let's assume that the controller knows actual currents supplied to Bus 1 shown as 'Ibus1a', 'Ibus1b' and 'Ibus1c' for the sake of understanding the concept of proposed scheme. Similarly, based on current inflows/outflows as shown in Figure 2.4 the expression of KCL at Bus 1 can be determined using Equation 2.6:

$$KCL_{\text{Bus1}} = I_{\text{Bus1}} - I_{\text{Line12}} - I_{\text{Load1}} \quad (2.6)$$

where,

KCL_{Bus1} represents the KCL at Bus 1.

I_{Bus1} represents the current flows incoming to Bus 1.

I_{Load1} represents the three-phase load current phasors reflecting current consumed by Load 1.

I_{Line12} represents the three-phase current phasors calculated previously.

Nonetheless, we can say that for steady state, the line currents entering a particular node is equal to the line currents exiting that node for all buses in the system. In simple words, the three-phase line currents I_{Line12} leaving Bus 1 will be exactly equal to the line currents entering Bus 2. Therefore, the three-phase line currents phasors calculated from Equation 2.2 exactly reflects the line currents flowing from Bus 1 to Bus 2 in steady state. That's why KCL would be zero at both Bus 1 and Bus 2 in the system for steady state. This observation needs to be analyzed when there is a fault present on the particular feeder between these two Buses.

2.5 Application of KCL for a Faulted Feeder

Consider a three-phase fault has occurred on the feeder between Bus 1 and Bus 2 as shown in Figure 2.5. The fault currents are represented as I_{fa} , I_{fb} and I_{fc} at the the faulted point voltages of V_{fa} , V_{fb} and V_{fc} as shown in Figure 2.5.

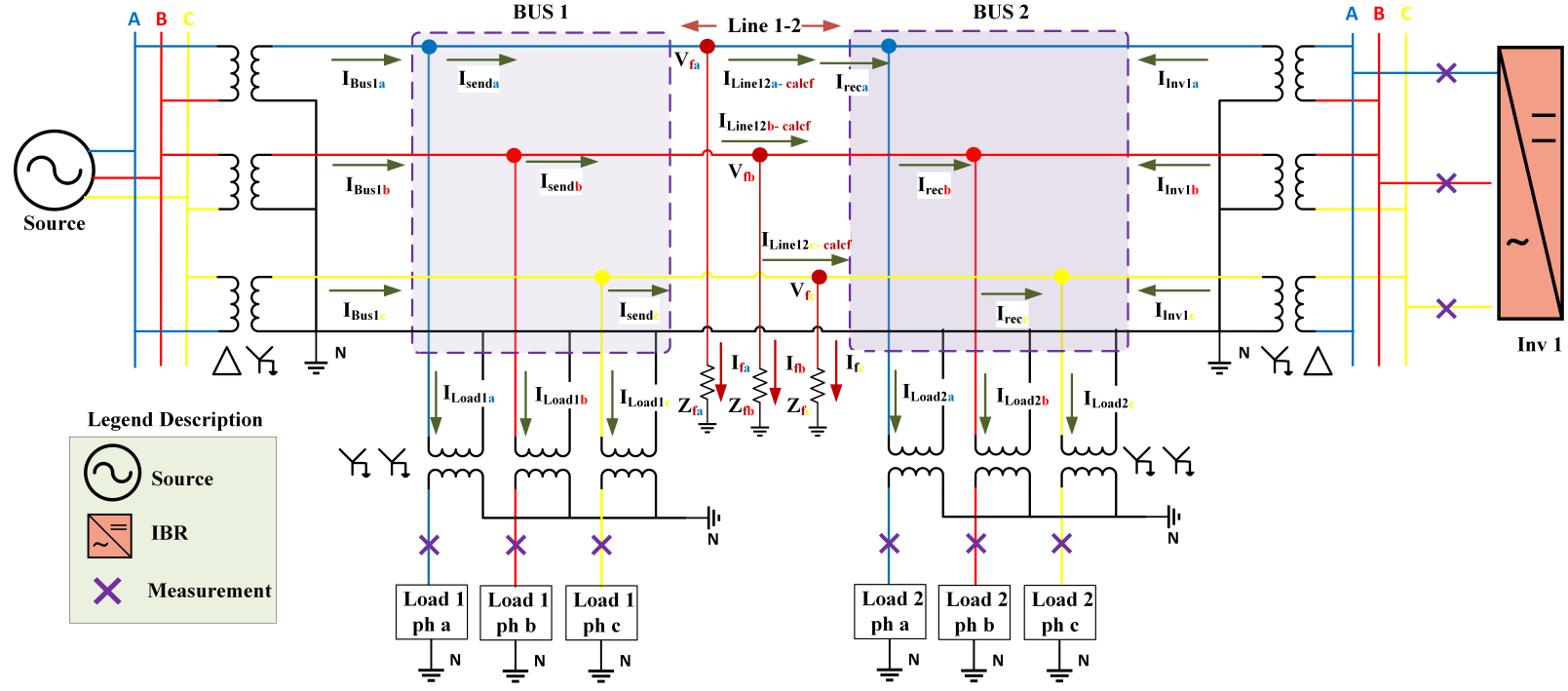


Figure 2.5: Current Flows for the System shown in Figure 2.3 During Fault

Figure 2.5 shows both the 'actual' current inflows/outflows as well as the 'calculated' current for the (feeder 1-2). The calculated currents are represented by $I_{\text{Line12a-calcf}}$, $I_{\text{Line12b-calcf}}$ and $I_{\text{Line12c-calcf}}$ to distinguish it from other currents in the system. For the required explanation in this section, the calculated line current is written as $I_{\text{Line12-calcf}}$ short for all three-phases.

Note that, $I_{\text{Line12-calcf}}$ is still calculated using previous **Equation 2.2** by taking into account the inverse of line parameters (Z_{Line12}) and the difference MV voltages at Buses 1 and 2 ($MV_{\text{Bus1}} - MV_{\text{Bus2}}$).

As seen in Figure 2.5, at fault instant, the three-phase line currents leaving Bus 1 will not be equal to the line currents entering Bus 2, unlike steady-state. This is because of the mismatch of currents between the sending end (from Bus 1) and the receiving end (to Bus 2) created due to the presence of a three-phase fault on the feeder. Here, the sending-end currents from Bus 1 are the actual fault currents shown as I_{fa} , I_{fb} and I_{fc} in Figure 2.5.

Therefore, unlike the steady state, the three-phase line currents phasors calculated from

Equation 2.2 no longer represent the actual line currents flowing from Bus 1 to Bus 2. In other words, the line current phasors calculated from Equation 2.2 during fault do not represent either the sending or receiving currents. It does not even represent the actual fault currents I_{fa} , I_{fb} and I_{fc} in this case. Therefore, the line current phasors calculated from 2.2 at the fault instant could be regarded as fictitious currents that are not 'actually' present anywhere in the system.

Now, based on the calculated line currents $I_{Line12-calc}$ during the fault, the controller computes KCL at Bus 2 in the same manner as shown in expression 2.7

$$KCL_{Bus2} = \boxed{I_{Line12-calc}} - I_{Load2} + I_{inv1} \quad (2.7)$$

where,

KCL_{Bus2} represents the (3x1) matrix of the KCL computed at Bus 2 during fault.

$I_{Line12-calc}$ represents the (3x1) matrix of three-phase current phasors calculated during fault.

I_{Load2} represents the (3x1) matrix of three-phase current phasors calculated during fault.

I_{inv1} represents the (3x1) matrix of three-phase current phasors calculated during fault.

Note that, the method of the computation of KCL at Bus 2 remains exactly the same regardless of the state of the system. However, the result of KCL would be different depending whether a fault is present on the system or not.

Let's assume that the controller knows actual currents supplied to Bus 1 shown as 'Ibus1a', 'Ibus1b' and 'Ibus1c' for the sake of understanding the concept of proposed scheme. Similarly, based on current inflows/outflows as shown in Figure 2.5 the controller computes KCL at Bus 1 from expression 2.8

$$KCL_{Bus1} = I_{Bus1} - \boxed{I_{Line12-calc}} - I_{Load1} \quad (2.8)$$

where,

KCL_{Bus1} represents the KCL at Bus 1 during fault.

I_{Bus1} represents the current flows incoming to Bus 1 during fault.

I_{Load1} represents the three-phase phasors of load current consumed by Load 1 during fault.

$I_{Line12-calc}$ represents the three-phase current phasors during fault.

Note that $I_{Line12-calc}$ is boxed out in both expressions for the computation of KCL at both

Bus 1 and Bus 2 because it is the set of only three-phase current phasors that does not represent the actual currents of the system during fault. That is why the term 'calc' has been added to distinguish it from other calculated currents. To elaborate, the other calculated currents, including load currents from **Equation 2.4** and inverter currents from **Equation 2.3**, represent the actual currents either consumed or supplied to the system even during fault. However, due to the accounting of $I_{\text{Line12-calc}}$ in the computation of KCL at Bus 1 and Bus 2, KCL will not be zero anymore at both Buses, unlike the steady state. In other words, KCL will not be satisfied either at Bus 1 or Bus 2 due to the calculation of three-phase line currents based on **Equation 2.2** during fault. This observation is utilized to locate the faulted feeder of the system, which will be explained further in the next chapter. Moreover, it will also be leveraged as part of the complete algorithm for identifying faulted feeder for any distribution system.

2.6 Summary of Chapter 2

This chapter presents the basic concept of the proposed protection scheme. As the FLISR protection scheme is developed for MV systems, converting phasor quantities onto the primary side of a distribution transformer based on the synchronized measurements received from the secondary side becomes necessary. Based on this, the calculation of three-phase, MV voltage and current phasors is explained using an example of a simple distribution system. Besides that, the rationale behind the expression for calculating three-phase line current phasors was also described in detail. Moreover, the process of computing KCL from calculated three-phase line current phasors was explained for a given bus. Lastly, the results of KCL on both buses of the system were analyzed and compared during steady-state and fault. The KCL was satisfied at both buses in the system's steady state. However, during fault, KCL was not satisfied on both Buses between which the fault was present on the feeder. This happened because calculated line current phasors do not represent the actual currents flowing from one bus to another during fault. The next chapter discusses the identification of faulted feeder based on this observation.

Chapter 3

Methodology

In this chapter, the basic methodology of the proposed protection scheme is described, which includes the following:

1. Detection of Fault
2. Identification of Fault (Type of Fault)
3. Location of Faulted Section

The FLISR methodology explained in this chapter can also be applied to any other renewable-fed distribution system.

Based on the concepts presented in this chapter, following the discussion on relay design in the next chapter, a complete overview of algorithms related to fault detection and identification, as well as the location of the faulted feeder, is presented at the end of the next chapter.

3.1 General Methodology

Figure 3.1 depicts general methodology to achieve FLISR for a system. The input to the relay of the central controller is low-voltage phasors, including three-phase voltages (V_{LVabc}) and three-phase currents (I_{LVabc}) from the secondary side of all distributed loads and from the delta side of IBRs interfacing transformer as described in the previous chapter.

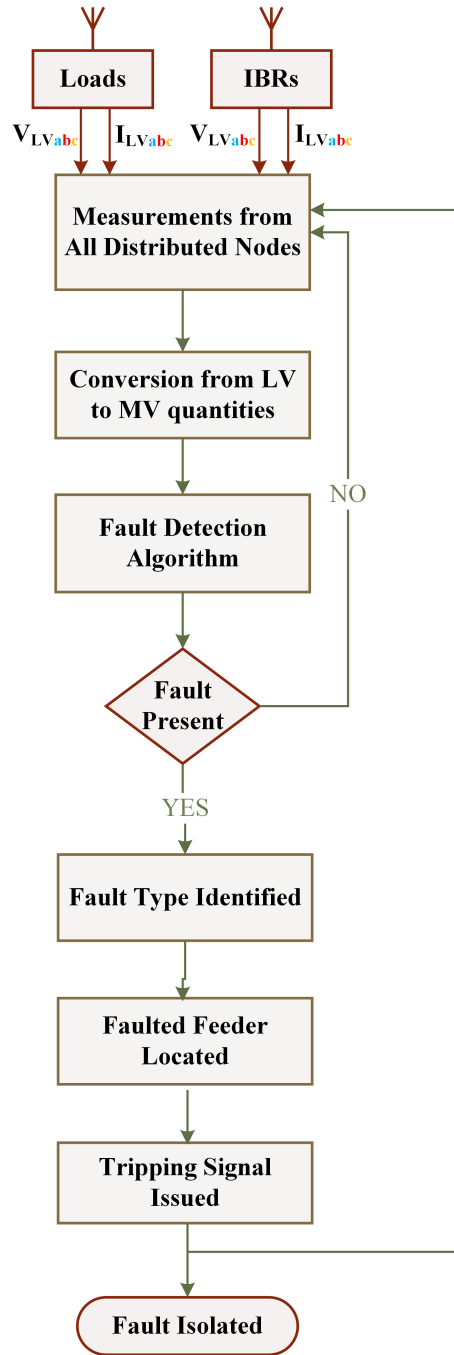


Figure 3.1: General Overview of FLISR Scheme

Then, low-voltage phasors are converted to medium-voltage phasors ($2401.8 V_{rated}$ for each phase) using Equation 2.1 explained previously. When a fault is present on the system, the fault detection algorithm acknowledges the presence of a fault on the MV system. Then, based on this

information, the identification of the type of fault and location of the specific faulted feeder is determined.

This information can be remotely transferred back to the appropriate protective device to isolate the faulted feeder in real-time. However, the tripping of appropriate protective device is out of the scope of this work.

3.2 Fault Detection

The complete algorithm for the detection and identification of fault is shown in Figure 4.1. Here, the methodology related only to the detection of fault on the MV system is explained:

3.2.1 Change in ΔV

As discussed before, three-phase LV phasors are converted to three-phase MV phasors ($2401.8 V_{rated}$ for each phase) using Equation 2.1. The same expression could be used to calculate three-phase, MV voltage phasors at all Buses in the system. Based on the determined MV voltage phasors in previous step, relay consistently computes the change in phase voltages (ΔV) from steady state to detect the presence of any transient on the system, including fault. So, when a fault occurs on the system, the voltage of the whole system drops down which is dominated purely by the physics of the system. Therefore, the value of (ΔV) becomes significant for the faulted phase(s) depending on the fault type. In this case, the threshold for (ΔV) is 20 Volts for each phase at which the relay enters the waiting period for testing the presence of a fault.

After the threshold for (ΔV) is met, the controller does not issue a tripping signal instantaneously as it will compromise the security of the protection scheme. That is why the controller's relay only operates in the presence of a permanent fault rather than any short-term transient. Therefore, a certain waiting period is required for the relay to operate reliably. This is further explained in Chapter 4 in Section (Wait-time of Relay).

3.2.2 Boundary Conditions

If the phasors reflecting the fault quantities still exist after the wait time is over, it implies the presence of a permanent fault on the system. After that, controller analyzes faulted phases (a, b, c) based on the following two boundary conditions.

3.2.2.1 First Boundary Condition

Depending on which of the three phases is faulted, the effect of the drop in voltage for that particular phase will be reflected for every Node of the MV system. For instance, when an Ag fault occurs on the MV system, the (a phase to ground voltage) will be lowered significantly compared to (b phase to ground voltage) and (c phase to ground voltage). The same effect will also be observed when all three phases of the system are faulted. Therefore, to determine which of the phases is faulted, a user-defined threshold is set to distinguish between the faulted and un-faulted phases of the MV system. On a healthy system, the voltages cannot be below *0.95 per unit*, so the threshold is set according to the nominal voltage, while providing some leverage for system dynamics, like load switching in the system. This threshold may vary from one system to another depending on the system scale. Therefore, for this study, a threshold of **0.8 per unit** is set to distinguish between faulted and un-faulted phases of the system safely.

The decision of the first boundary condition is analyzed based on the following expressions, which test the drop in voltage magnitude for each phase below the set threshold of 0.8 per unit:

$$Decision_{\text{phase a}} = MV_a < Threshold \quad (3.1)$$

$$Decision_{\text{phase b}} = MV_b < Threshold \quad (3.2)$$

$$Decision_{\text{phase c}} = MV_c < Threshold \quad (3.3)$$

If the first boundary condition is met, the fault on the MV system is confirmed. After this, the type of fault and location of the faulted feeder can be identified simultaneously.

3.3 Fault Identification

The identification of the type of fault depends on the second boundary condition and the computation of zero-sequence voltage, which are explained as follows.

3.3.1 Second Boundary Condition

The second boundary condition does not depend on any user-defined threshold but on the relative comparison of line-to-line voltages (V_{ab} , V_{bc} , V_{ac}). The line-to-line voltages are calculated as:

$$V_{ab} = V_a - V_b \quad (3.4)$$

$$V_{bc} = V_b - V_c \quad (3.5)$$

$$V_{ca} = V_c - V_a \quad (3.6)$$

The line-to-line voltages are the difference between two phase to ground voltages. This fact can also be utilized to determine the faulted phases. For instance, when an Ag fault occurs on any system, both V_{ab} and V_{ac} will be relatively much lower as compared to V_{bc} . Similarly, when an AB or ABg fault occurs on the system, V_{ab} will have the lowest magnitude as compared to the magnitude of V_{bc} and V_{ac} . This relative comparison further confirms faulted and un-faulted phases without setting a user-defined threshold. .

3.3.2 Zero-Sequence Voltage

When faulted phases are identified, the next step is to determine the nature of the fault. That is, whether a fault is a ground fault or a line-to-line fault. The best factor to distinguish between ground faults and line-to-line faults is zero-sequence voltage, which is calculated as follows:

$$V_0 = \frac{1}{3} \times (V_a + V_b + V_c) \quad (3.7)$$

The zero-sequence voltage would be negligible for a line-to-line fault (for example, AB fault) on the system, as the ground circuit is incomplete. On the contrary, when there is a ground fault (for instance, ABg fault), the zero-sequence voltage will be significantly higher than a line-to-line fault. This information is utilized by the controller's relay, which calculates zero-sequence voltage, particularly when two system phases are faulted simultaneously. This condition is applied right

after determining faulted phases, when the wait time for relay operation is over, and the above two boundary conditions are checked. It should be noted that for a highly unbalanced system, like IEEE 13 Bus, the quantity of zero-sequence voltage would not be precisely zero even during the system's steady state. Therefore, the threshold for distinguishing between line-to-line and ground faults should be set accordingly. In this case, Bus 632 is taken as a reference for the calculation of zero-sequence voltage for every type of fault on the system. The threshold is set at 10 Volts. So, for ground faults, the zero-sequence voltage will be significantly higher than the set threshold.

3.4 Faulted Feeder Location

The algorithm of finding the faulted line/feeder/section is executed right after fault detection by the central controller.

Figure 4.2 shows the complete algorithm for the faulted feeder identification. Here, only the methodology of the location of the faulted feeder for the IEEE 13 Bus system is explained, which is taken as a test system for simulation in this report. The required data for the IEEE 13 Bus system is already available at [25], including feeder parameters used to calculate three-phase line current phasors, as described in the previous chapter. Thus, the three-phase current phasors for all the lines of the system are determined at fault instant using Equation 2.2

3.4.1 Concept of Intersection Bus and Connected Bus

Once the three-phase MV phasors at all Buses and three-phase currents for all feeders at the time of fault are known, the algorithm analyses the voltage drop for every area in the system. An area is a group of Nodes connecting two or more lines in the system. For an area, there is a main Intersection Bus and its Connected Bus/Buses. An intersection bus connects one or more outgoing feeders, whereas connected buses are linked to outgoing feeders connected to the intersection bus.

For example, in Figure 3.2, Bus 632 is an Intersection Bus linked with the outgoing feeders of Bus 633, Bus 645 and Bus 671, which are its Connected Buses. This comprises Area 1. Similarly, Bus 671 is an Intersection Bus, whereas Bus 692, Bus 684 and Bus 680 are its Connected Buses. This includes Area 3. It is also possible that the Intersection Bus of one Area could be the Connected Bus of another Area. For example, Bus 645 is the Connected Bus of Area 1, whereas it is an Intersection Bus of Area 2.

Figure 3.2 highlights all Areas considered for IEEE 13 Bus system in this algorithm.

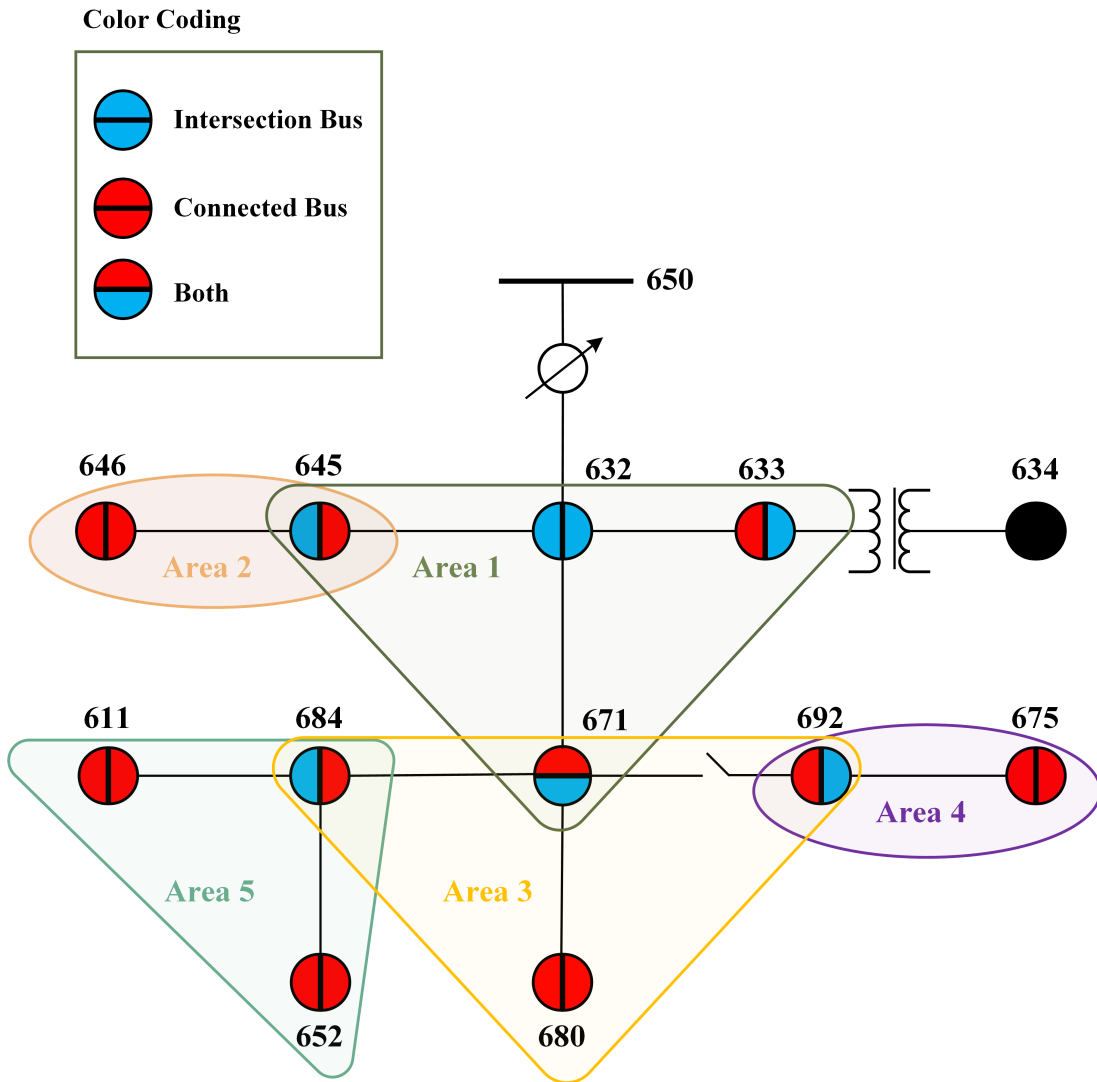


Figure 3.2: Areas of IEEE 13 Bus System

3.4.2 Voltage Drop of Faulted Area

When a fault occurs on the system, the buses closer to the faulted feeder which comprises an area are likely to have more voltage drop than the buses in another area. This fact could narrow down the faulted section, especially in more extensive systems with several buses.

However, the drop in voltage magnitude cannot be an absolute indicator in identifying the faulted feeder section. It is possible that the buses adjacent to the faulted feeder can have more

voltage drop than the buses between which the fault is present. For instance, consider a two-phase fault occurs at 95 % feeder length between Buses 645 and 646. It is very possible that for extreme lengths, as in this case, Bus 632 and Bus 645 can have relatively more voltage drop than Bus 645. This could lead to misidentification of the faulted feeder. Based on this, other checks are needed to identify the faulted feeder correctly

3.4.3 Identification of Faulted Feeder

Most helpful check in identifying the faulted feeder is the computation of (KCL) at each node. As discussed in the previous chapter, the line currents entering a particular node are equal to the line currents exiting that node in a steady state of the system. That's why KCL is zero at all Buses of the system in a steady state.

Now, consider a three-phase fault that occurs at 50 % line length between Bus 632 and Bus 633. Based on the previous discussion in Chapter 2, the calculated three-phase currents phasors from Equation 2.2 represent the actual currents flowing through all the lines *except for the feeder where the fault is present*. In this case, this feeder is 'Feeder 632-633'. Therefore, at fault instant, the calculated line currents entering and leaving all system buses during the fault will be exactly the same except for Bus 632 and Bus 633. Here, the mismatch of calculated and actual line currents for Feeder 632-633 is caused by the presence of another current path created due to fault. Therefore, the KCL will not be satisfied at Bus 632 and Bus 633. However, it will be satisfied at the remaining buses of the system between which the fault is not present on the feeder. This information is sufficient to identify the faulted feeder for any system regardless of the number of buses, infrastructure and nature of sources.

The next chapter presents the complete faulted feeder identification algorithm based on this.

3.5 Summary of Chapter 3

This chapter presents a general overview of the methodology of the FLISR scheme. Besides that, the basic method for detecting and identifying the type of fault was explained. This included the computation of (ΔV) by the controller consistently, two boundary conditions regarding the drop in MV voltages below a set threshold (**0.8 per unit**) for fault detection as well as relative comparison of line-to-line voltages for the identification of faulted phases. Moreover, the quantity

of zero-sequence voltage was utilized to determine the nature of fault - faults with/without ground. Finally, the basic methodology for the location of faulted feeder was explained, which included the concept of intersection and connected bus for a system, voltage drop for a faulted area and lastly, the identification of faulted feeder during fault.

Chapter 4

Relay Design and Algorithm

This chapter discusses essential relay design and testing parameters that make the FLISR scheme possible. Therefore, this chapter extends the FLISR methodology explained in the previous chapter. Lastly, the complete overview of algorithms relating to fault detection and identification, as well as faulted feeder location, is presented with the assistance of flowcharts.

4.1 Important Parameters of Relay Design

Following section involves the overview of important parameters of Relay design which are required for the implementation of FLISR.

4.1.1 Sampling Rate

The conventional numerical relays consist of an analog anti-aliasing filter, which removes the high-frequency components before obtaining digital samples for phasor estimation. However, modeling an analog filter in a digital simulation like RSCAD is not possible. Therefore, the ideal way is to sample the signals at a very high sampling rate that leaves no chance of anti-aliasing behind. According to [26], a sampling rate of 48 kHz has been tested to completely remove the need for an anti-aliasing filter. However, the sampling rate of 48 kHz puts a high computational burden on the cores of the RTDS. Therefore, an optimal choice of sampling rate should be made to complement both the anti-aliasing and low computational power of the simulator. After performing studies and comparing phasor estimates of 48 kHz and 16 kHz, it was noted that errors for three-phase voltages

are ± 1.5 Volts and ± 2 Amps for three-phase currents. For the purpose of this analysis, these errors are acceptable for reducing the computational burden on the digital simulator. Therefore, the sampling rate of **16 kHz** was selected (16,666 phasors/sec) in this study for phasor estimation.

4.1.2 Wait-time of Relay

As discussed in the previous chapter, the relay consistently receives synchronized phasors of three-phase voltage and current from all LV Distributed Nodes of the system in each cycle. This means, that 278 phasors/cycle are processed by sliding window of DFT in each fundamental cycle. As discussed previously, there is a certain waiting period required for the relay to operate in a reliable manner. Therefore, the reliable yet optimal waiting period of the relay needs to be determined before a fault is declared on the MV system.

Since at the occurrence of a fault, the obtained phasors do not accurately represent fault quantities because of the presence of pre-fault samples in sliding window of DFT. That is why, all legacy relays wait for at least one fundamental cycle $16.67ms$ [27]. However, this is only the minimum time of operation, not the total wait time of relay. In this study, only 8 out of 278 phasors are sent from LV sensors/ (IEDs) to the relay so that the communication channels are not overburdened. This was also mentioned previously in Chapter 1 for the requirements of LV sensors/devices. Note that, these 8 phasors are equally spaced over a cycle, which means one phasor is obtained after every $\frac{1}{4}$ cycle.

After the waiting period of one fundamental cycle is completed, the relay waits till it gets two consecutive phasors of the same value (lower than the threshold of 0.8 per unit), which implies that the DFT window is now filled with only fault samples, and then waits for another two more phasors having relatively same value (within a small tolerance) for security before declaring a fault. This turns out to be approximately $\frac{1}{2}$ cycle, which is the waiting period of four consecutive phasors processed by the relay after the completion of the fundamental cycle. To calculate the overall wait time, this delay of $\frac{1}{2}$ cycle must be added to the minimum time of operation of relay.

Therefore, in this study, the total waiting period of relay includes time of 1 fundamental cycle, and $\frac{1}{2}$ cycle. This yields the total wait-time of $25ms$ that is, 417 samples before testing the presence of fault on the system. In other words, the relay holds off any operation till 417 phasors are passed even after the threshold for (ΔV) is met. That's why a 'TRIGGER' is shown Figure 4.1 after wait time of relay without which, the relay does not even check the first boundary condition.

If the phasors reflecting the fault quantities still exist after the wait time, it implies a permanent fault on the system.

4.2 Overview of Algorithm for Fault Detection and Identification

Figure 4.1 shows all the steps which are sequentially executed by the algorithm of Fault Detection and Identification.

First, the relay consistently calculates three-phase, medium-voltage phasors from Equation 2.1 and computing (ΔV) each fundamental cycle. At any instant, if (ΔV) is increased more than the set threshold, which is taken as 20 V in this study, the relay enters the waiting period. After the waiting period of $25ms$ is over, the relay analyses the first boundary condition for each phase using expressions: 3.1, 3.2 and 3.3 discussed in the previous chapter. If the magnitude of any medium-voltage phase is found below the set threshold, which is taken as **0.8 per unit** in this study, the relay declares the presence of a fault. At this point, the relay has acknowledged the presence of fault on the MV system.

After the first boundary condition is satisfied, the identification of faulted phases and the location of the faulted feeder is done simultaneously. For the identification of faulted phases, the second boundary condition is analyzed given in expressions: 3.4 , 3.5 and 3.6 from the previous chapter. Once the faulted phases are identified, the type of fault can be determined using the quantity of zero sequence voltage, which can be calculated using Equation 3.7. Based on this, any fault can be detected and identified, whether with ground (SLG, LLG fault) or without ground (LL, LLL fault).

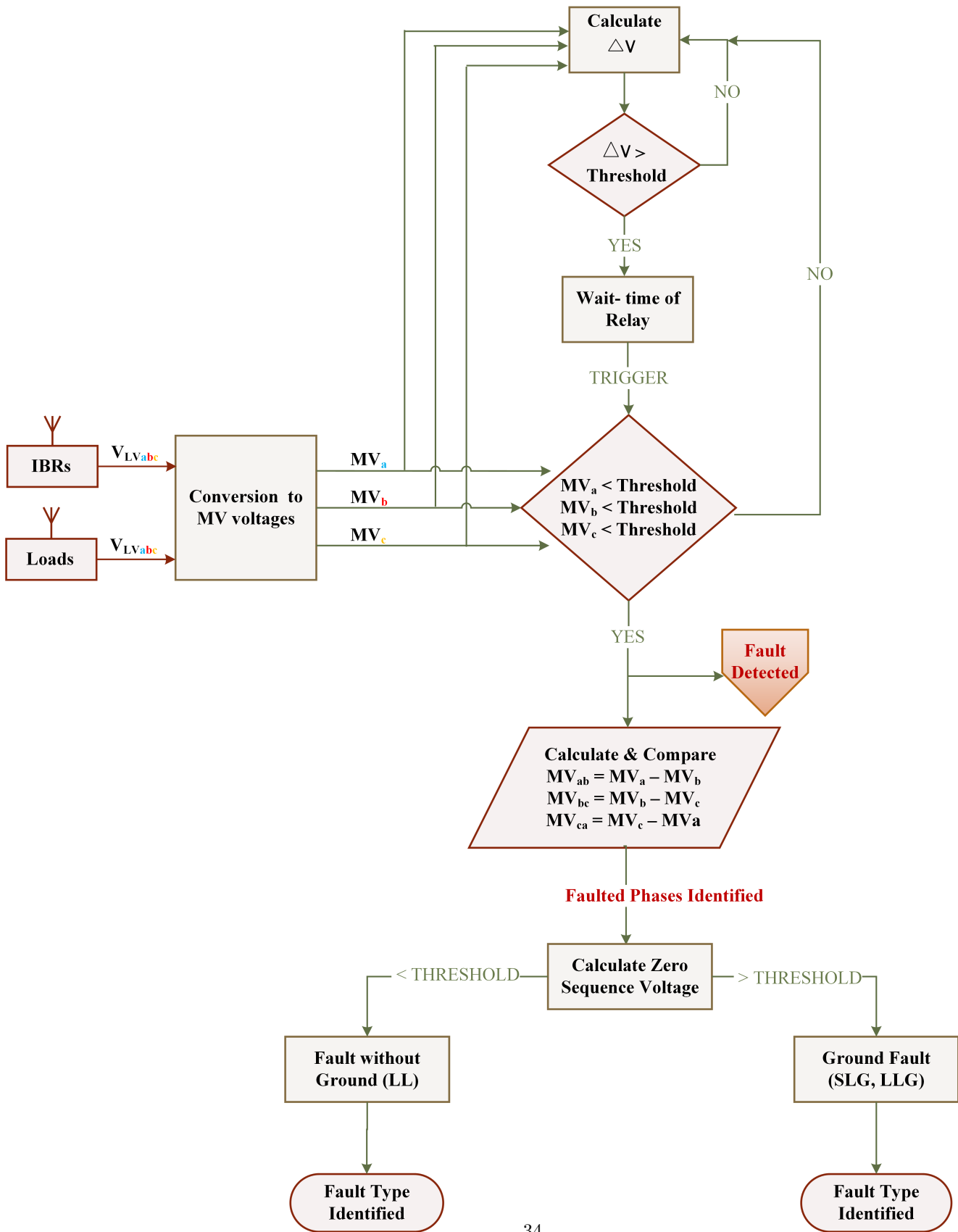


Figure 4.1: Algorithm for Fault Detection and Identification

4.3 Overview of Algorithm for Faulted Feeder Location

Figure 4.2 shows all the sequential steps which are executed by the algorithm of faulted feeder identification .

In summary, the faulted feeder is identified after fault detection. That is why an off-page reference named 'Fault Detected' is used as a remote connector for localization of the faulted feeder, as shown in Figure 4.1. Three-phase MV voltages at all buses is calculated using Equation 2.1. Then, three-phase line currents are calculated using Equation 2.2. Similarly, three-phase primary load and inverter currents are computed considering their respective transformer's turns ratio and phase shift.

First of all, the algorithm identifies the Area that has a relatively higher voltage drop than other areas. Then, the relay computes the KCL at the Intersection Bus of that particular Area. The violation of KCL at Intersection Bus of the Area implies a fault present on any of the Area's outgoing feeder(s). Secondly, KCL is computed at any of the Connected Bus/Buses of the Area. If KCL is violated at the Connected Bus as well, it means that the feeder between the Intersection Bus and Connected Bus is the faulted feeder. Otherwise, the algorithm moves to other Connected Buses and computes KCL again. It keeps on doing this, until it finds the Connected Bus where KCL is not satisfied. That's how it tracks down the faulted feeder.

On the contrary, if KCL is satisfied for the intersection bus of an area, the algorithm moves to another area with a relatively lower voltage drop and computes KCL at the intersection bus of that Area. It keeps on doing this until it finds the Intersection Bus where KCL is violated. The rest of the process remains the same.

For an example, consider a two-phase fault that has occurred at 95 % feeder length between Bus 645 and Bus 646. As mentioned before, it is possible that Area 1 might have relatively more voltage drop as compared to Area 2. Now, pay attention to the sequential steps taken by the algorithm to track down the faulted feeder. As a first step, the algorithm identifies the Area having the most voltage drop, which is Area 1 in this case. After calculating three-phase MV voltages, line currents, load and inverter currents, the algorithm computes KCL at Bus 632, the Intersection Bus of Area 1 (See Figure 3.2). As no fault is present on any of the outgoing feeders of Area 1, KCL will be satisfied. Therefore, the algorithm moves to the Area having the most voltage drop, excluding Area 1. This is Area 2 in this case. After that, KCL is computed at the Intersection Bus of Area 2,

which is Bus 645. Now, the KCL will not be satisfied at Bus 645. This serves as a major reason to acknowledge the presence of fault on the feeder of Area 2. Since this is the only feeder of Area 2, KCL will be computed at the only Connected Bus of Area 2 as the next step, Bus 645. As expected, the KCL will not be satisfied at Bus 645 either, which further confirms the presence of a fault on the feeder between Bus 645 and Bus 646. That's how, even for extreme feeder distances, the algorithm tracks down the faulted feeder.

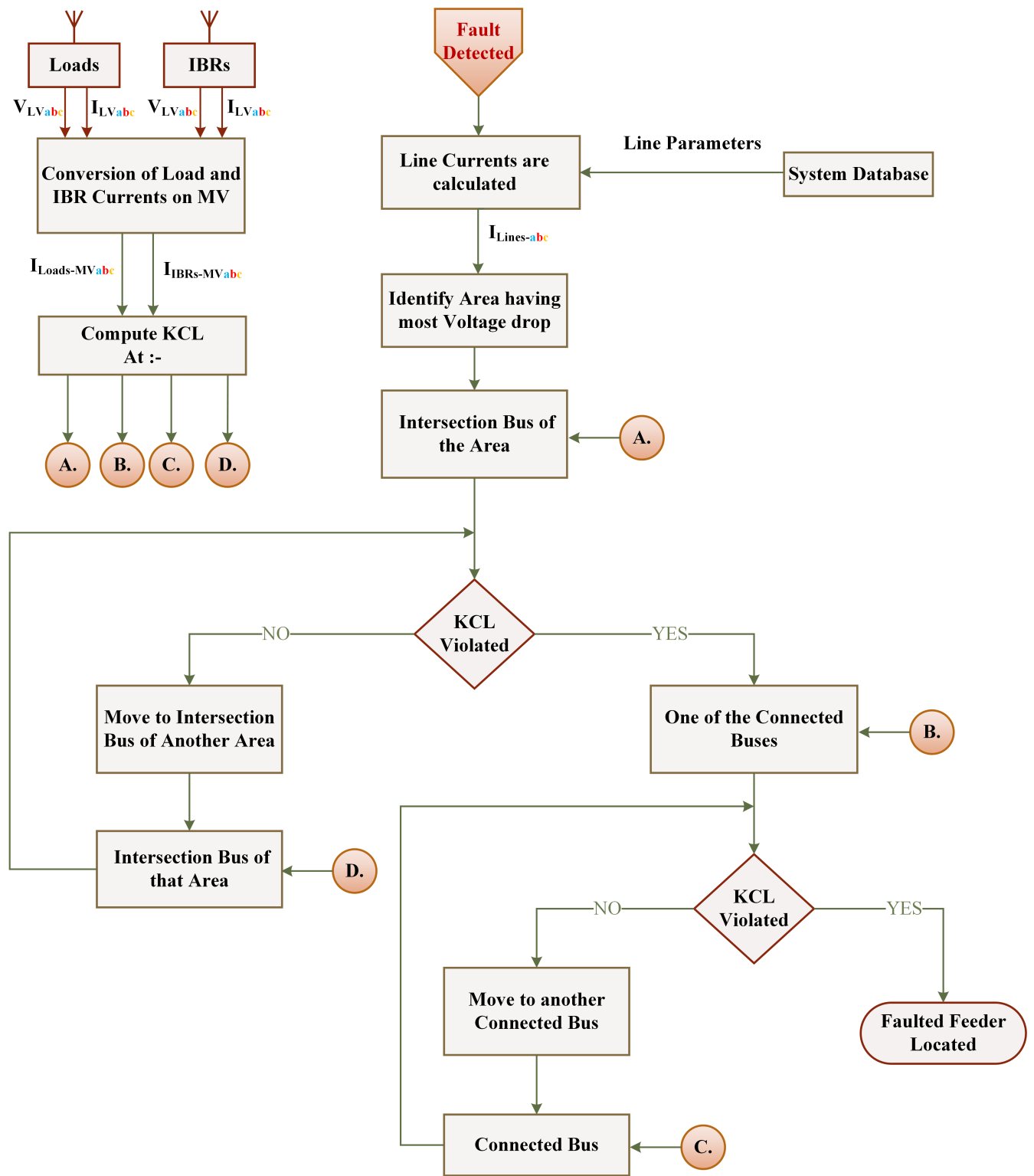


Figure 4.2: Algorithm for Location of Faulted Feeder

4.4 Summary of Chapter 4

In this chapter, the critical parameters of the design and testing of the relay were discussed, which is necessary for the implementation of the FLISR scheme. These parameters include the sampling rate and the wait time of the relay. The sampling rate of **16 kHz** was selected for phasor estimation. The total waiting period of the relay was determined to be $29ms$, after which the first boundary condition is checked. Following this discussion, an overview of algorithms for both fault detection and identification, as well as the location of the faulted feeder, was explained with the help of flowcharts.

Chapter 5

Test System

One of the benchmark systems IEEE offers for testing and analyzing distribution systems is the IEEE 13 bus feeder employed for this study. The single-line diagram of the IEEE 13 Bus feeder is shown in Figure 5.1

IEEE 13 Bus System is a highly unbalanced system rated at 4160 V with unbalanced loading, shunt capacitors, overhead and underground lines, making it an ideal choice for the simulation of distribution systems. According to the data available at [25], a 5MVA, 115kV/4.16kV, (Δ - Y_g) transformer with an impedance of $0.01 + j0.08$ per unit is used as the substation transformer. An ideal source rated at 115 kV represents the main grid. Typically, the grid would have a 10 to 15% Thevenin positive sequence impedance on a 100 MVA base. Due to the transformer connection, the zero sequence impedance of the ideal source is isolated. However, this system's substation transformer impedance greatly influences the grid impedance. Therefore, this work is not greatly affected by grid impedance. Additional information about the load data and system metrics is provided in [25].

5.1 Distribution Line Model

Before analyzing a distribution feeder, it is essential to determine the series impedance for overhead and underground lines. Unlike high-voltage transmission lines, which are equally loaded (balanced loading), distribution lines are not transposed, making them unbalanced. Therefore, the series impedance of a three-phase distribution line comprises the self- and mutual impedance terms,

which also account for the ground return path for unbalanced currents [28]. This is reflected as a **Phase Impedance Matrix** obtained through Carson's equations and Kron reduction step. A general three-phase line segment model is shown in Figure 5.2. That is why the line parameters of a three-phase line shown in Figure 5.2 are taken as a (3x3) matrix for analysis, as described in Chapter 2. IEEE 13 Bus system provides parameters of the Distribution Line Model, that is, the phase impedance matrix for every system feeder. Figure 5.2 is reproduced from a book chapter in [28].

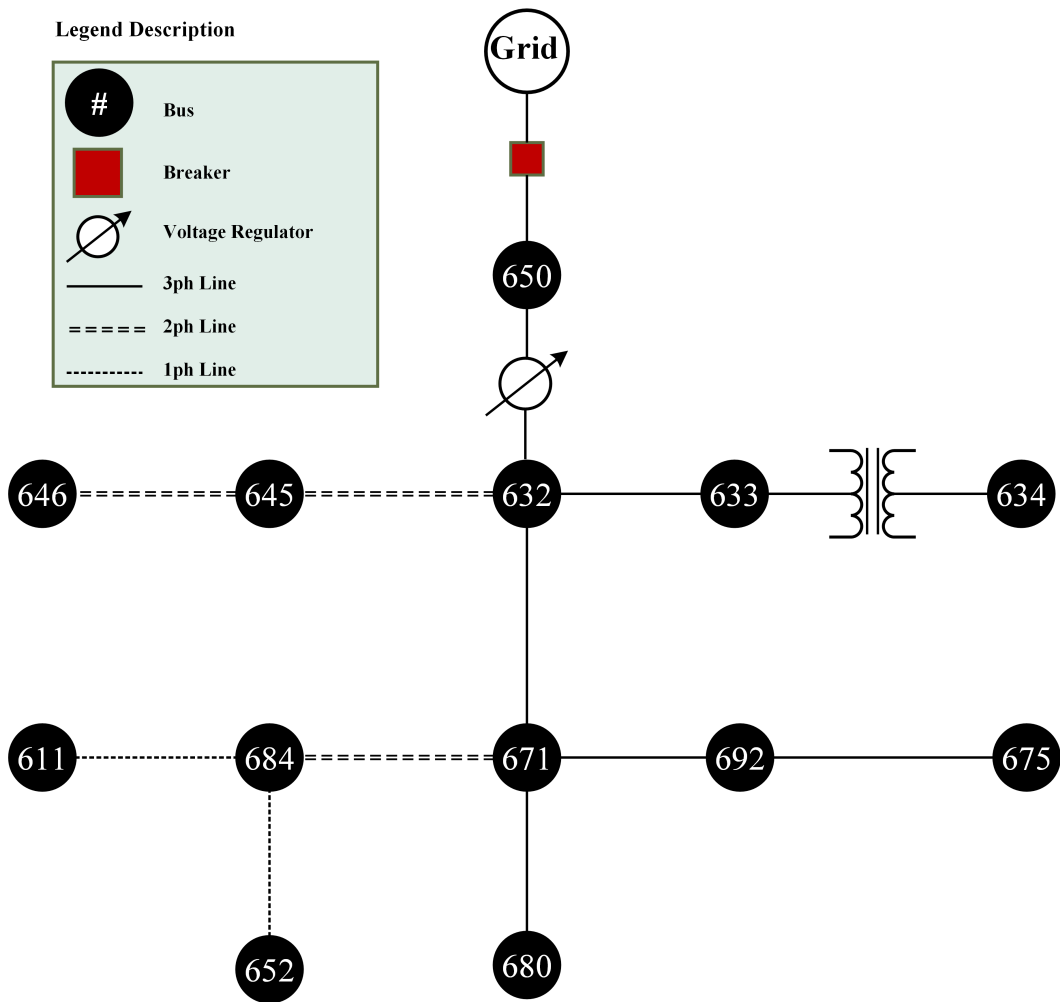


Figure 5.1: IEEE 13 Bus System

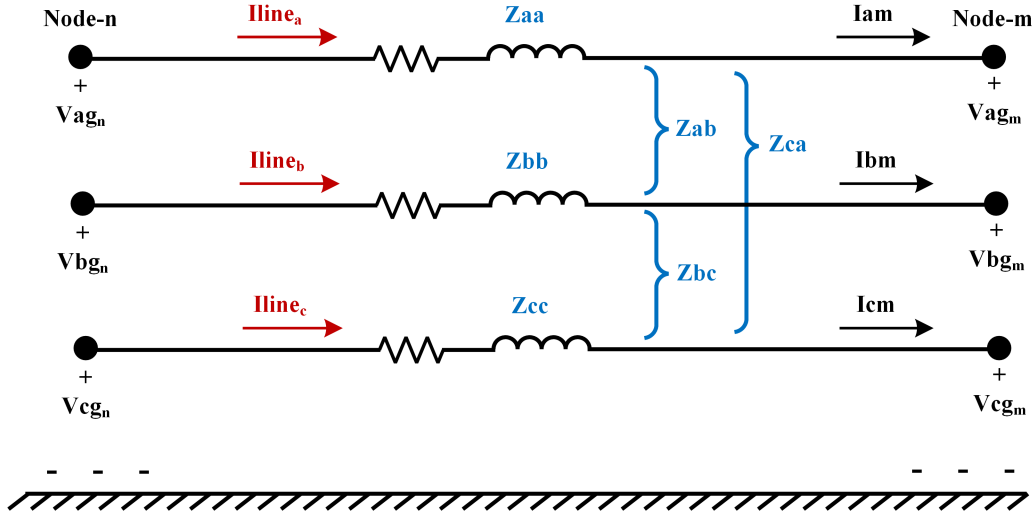


Figure 5.2: Three-phase Line Segment Model

5.2 Connection of Inverter Based Resources (IBRs)

In RSCAD, the test system design for IBRs is taken from [5]. To test the distribution system in the presence of IBRs, one grid-forming IBR rated at 1500 kVA and three grid-following IBRs rated at 1500 kVA, 1000 kVA and 800 kVA are connected to the system. All the IBRs are connected through 480V/4.16 kV, (Δ - Y_g) interfacing transformers at buses 650, 633, 675 and 680, respectively. The grid-forming IBR is connected at Bus 650, so it can act as an alternative supply source in islanded mode. Nonetheless, the total MVA rating of IBRs is selected to cover all the system loads plus losses. In grid-connected mode, all the grid-following IBRs operate in grid-following mode at constant power factor while grid-forming IBR at bus 650 remains OFF. That's why all the grid-following IBRs do not produce negative sequence currents in any mode of operation of microgrid. In islanded mode, the system voltages are balanced by grid-forming IBR, which provides both positive and negative sequence currents to the system. The rest of the inverters continue to operate in the same manner. According to IEEE Standard 1547 [29], all inverters can fault ride through (FRT) in reactive power priority mode. As discussed in the literature review, IBRs can only output a limited fault current. Therefore, a current injection limit of 1.5 pu and 1.2 pu is set for grid-forming and grid-following inverters. The inverter's precise design, modes of operation, and controls for this system are covered in depth in [5] and [30]. Figure 5.3 shows the single-line diagram of the modified

model after integrating IBRs in the IEEE 13 Bus system. This image is reproduced from [30] to show the specific connection of IBRs to the IEEE 13 Bus feeder.

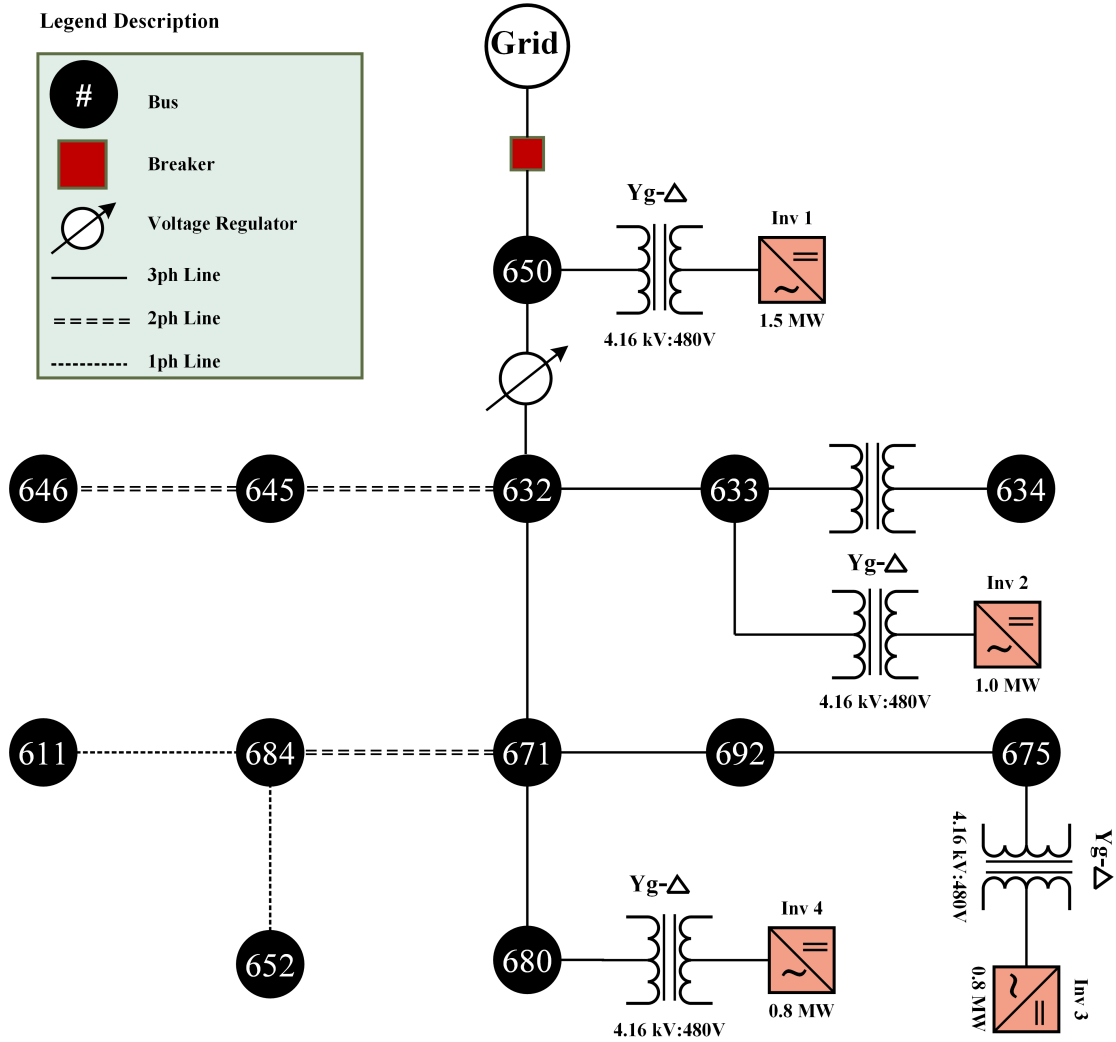


Figure 5.3: IBRs in IEEE 13 Bus System

5.3 Low-Voltage (120 V) Loads

The original IEEE 13 bus system has three-phase and single-phase loads modeled at medium voltage (4.16 kV). Nonetheless, the system includes constant impedance as well as other load types. As the proposed FLISR scheme is designed for MV systems using LV sensors, all the three-phase load measurements must be taken from the LV side, typically rated at (120V/240V) for residential

distribution systems.

Therefore, for this analysis, three-phase transformers rated at (4.16kV/208V) and single-phase transformers rated at (2.40kV/120V) were installed to respective feeder buses, and all MV loads were moved to the secondary side of connected transformers. In this way, the measurements of three-phase voltages and currents from LV, the secondary side of the transformer rated for (120 V) became possible, as described in Chapter 2.

However, the original MVA rating and load type remain unchanged to avoid affecting the system's overall loading. The connection for all three-phase transformers was taken as ($Y_g - Y_g$) for the ease of calculations as the conversion from LV to MV phasors for this connection yields 0° phase shift. The relation between transformer connection and associated phase shift is discussed in detail in Chapter 2. Nonetheless, the capacity of all transformers was selected based on the respective ratings of the loads they fed so that the transformers would not become overloaded at any point in time.

Important information regarding the rating, turns ratio, and percent impedance (% Z) for both three-phase and single-phase transformers installed at respective Buses in the original IEEE 13 Bus feeder is summarized in Table 5.1. The transformer impedance (% Z) is selected according to the guideline in [31], which provides a range of impedance (% Z) for low voltage dry type transformers based on their KVA ratings and connection (three-phase/single-phase). So, a typical value of the percent impedance (% Z) is selected from the range provided in Table 2 of guideline for each connected transformer [31].

Connection	Bus ID	Phases (a, b, c)	Rating (MVA)	Turns-Ratio (MV : LV)	(% Z)
Three-Phase	650	a, b, c	0.2 MVA	4.16 kV : 0.208 kV	5.0
Three-Phase	632	a, b, c	0.2 MVA	4.16 kV : 0.208 kV	5.0
Three-Phase	633	a, b, c	0.5 MVA	4.16 kV : 0.208 kV	6.0
Three-Phase	671a	a, b, c	0.2 MVA	4.16 kV : 0.208 kV	5.0
Three-Phase	671	a, b, c	3.1 MVA	4.16 kV : 0.208 kV	8
Three-Phase	680	a, b, c	0.2 MVA	4.16 kV : 0.208 kV	5.0
Three-Phase	692	a, b, c	1 MVA	4.16 kV : 0.208 kV	6.5
Three-Phase	675	a, b, c	1 MVA	4.16 kV : 0.208 kV	6.5
Single-Phase	645	b	0.3 MVA	2.40 kV : 0.120 kV	5.8
Single-Phase	645	c	0.3 MVA	2.40 kV : 0.120 kV	5.8
Single-Phase	646	b	0.3 MVA	2.40 kV : 0.120 kV	5.8
Single-Phase	646	c	0.3 MVA	2.40 kV : 0.120 kV	5.8
Single-Phase	684	a	0.3 MVA	2.40 kV : 0.120 kV	5.8
Single-Phase	684	c	0.3 MVA	2.40 kV : 0.120 kV	5.8
Single-Phase	652	a	0.3 MVA	2.40 kV : 0.120 kV	5.8
Single-Phase	611	c	0.3 MVA	2.40 kV : 0.120 kV	5.8

Table 5.1: Load Transformers Data

That is how the IEEE 13 Bus feeder shown in Figure 5.3 is further modified to include loads and transformers for all possible feeder phases and at each bus.

The detailed SLD of the final system with connected IBRs and LV loads is shown in Figure 5.4. This system represents a renewable-fed distribution system that can measure three-phase voltage and currents from the LV side (120V) to the central controller, as described in Chapter 2.

In the next chapter, the simulation and analysis of the proposed protection scheme will be conducted and examined on the Test System shown in Figure 5.4.

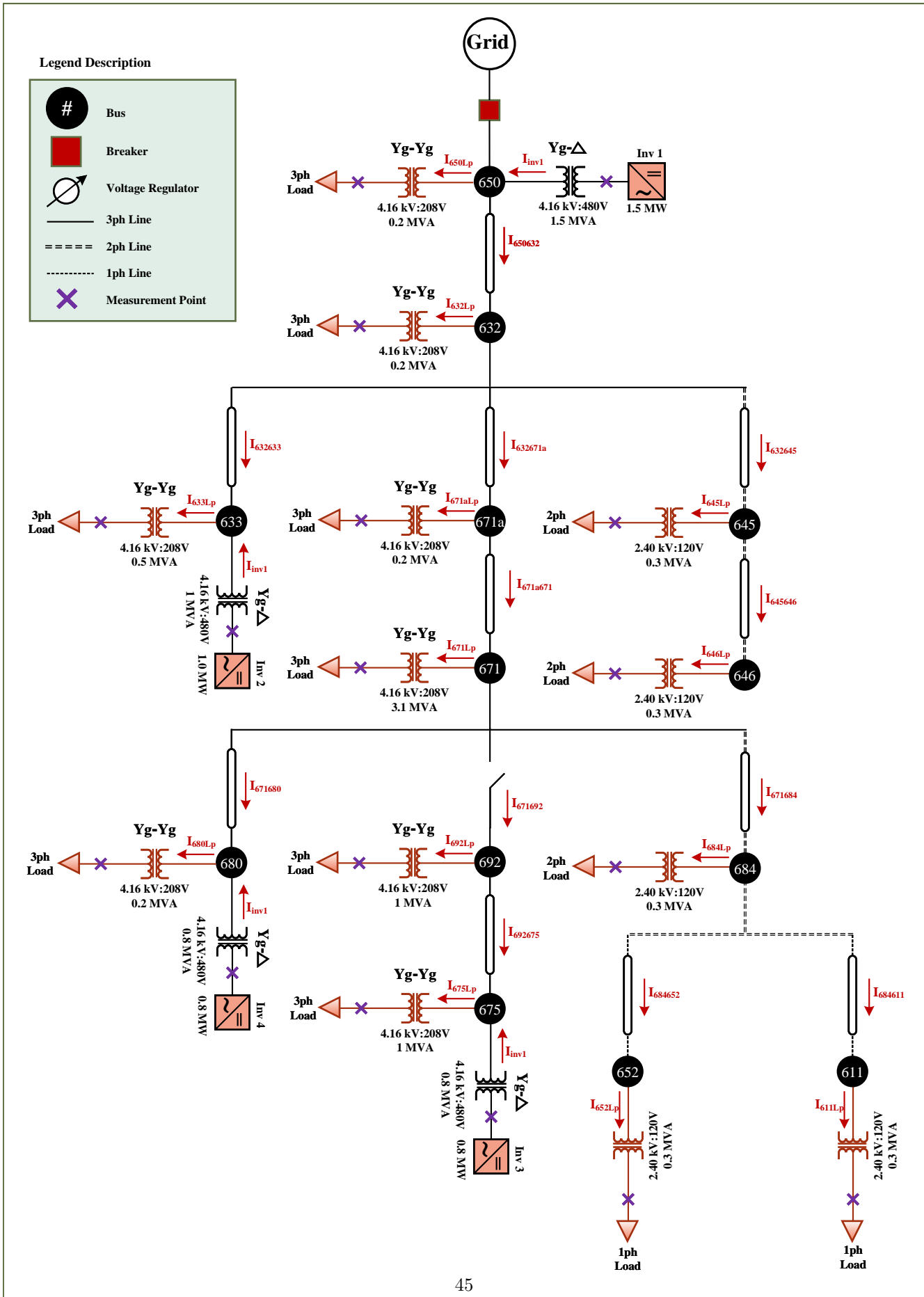


Figure 5.4: Final Test System

5.4 Computation of KCL expressions for the Test System

After obtaining the final Test System shown in Figure 5.4, the expressions of KCL at every system bus can be written. Appendix A shows the complete list of KCL equations for every bus of the Test System. The expressions of KCL are essential as the algorithm for identifying faulted feeder described previously in Chapter 4.

5.5 Summary of Chapter 5

The final test system for analyzing the proposed protection scheme is developed in this chapter. The modified system is based on the IEEE 13 Bus feeder, which has all the characteristics of a distribution system, including unbalanced loads and distribution lines. The design and control of connected inverters to the modified system is taken from [5]. A microgrid is formed by a combination of a single grid-forming IBR and three grid-following IBRs rated connected to the original IEEE 13 Bus system.

The system is further modified by transferring all MV loads rated for (4.16kV) to an LV, distribution voltage rated for (120V) by connecting three-phase and single-phase step-down transformers at respective buses. All installed transformers' capacity was selected according to load rating so that the transformers do not become overloaded. This system is the complete representation of a renewable-fed distribution system that can provide measurements of three-phase voltage and currents from the LV side (120V) to the central controller, as described in previous chapters. Finally, the final Test System for analyzing the proposed protection scheme is shown in Figure 5.4. In the next chapter, the simulation and analysis of the proposed protection scheme will be conducted and examined for the developed Test System.

Chapter 6

Simulation

6.1 Simulation Software

The simulation and modeling of this study is done on Electromagnetic Transient (EMT) platform in real time using RSCAD. This platform helped speed up the simulations with IBRs. Whereas, MATLAB is used for the coding of relay algorithm described in chapter 3 and 4.

RSCAD provides an extensive library of power and control components, scripting functions, and different IEEE benchmark systems, including the IEEE 13 Bus feeder, all utilized in this study. Therefore, RSCAD is adopted for the modeling of the Test system explained in the previous chapter.

The protection logic of the proposed protection scheme described in Chapter 3 is developed using MATLAB on a personal computer, which performs the job of a central controller to the system. Therefore, all the fault detection and identification algorithms and the faulted feeder's location are coded into MATLAB, which analyzes faults created in the RSCAD model in offline mode. The phasor estimates of the input measurements to the controller consisting of three-phase LV voltages and currents for the system shown in Figure 5.4 are obtained through cosine-filter DFT in RSCAD. Then, the obtained phasors are converted to appropriate MV phasors quantities in MATLAB, as described in Chapter 3. Finally, the determined MV phasors are tested and passed through the algorithms built in MATLAB for fault detection and identification and faulted feeder location as described in Chapter 4. All the phasor values from every distributed node of the described system are analyzed and tested immediately once the relay's waiting period from the fault's commencement is over in a synchronized manner.

Note that, the test system is analyzed and tested between these two simulation programs without accounting for the communication delay from RSCAD to MATLAB. Therefore, all the results described in this chapter pertain to the offline analysis of the system shown in Figure 5.4, which is simulated in RSCAD and examined in MATLAB based on the protection logic of the proposed protection scheme described in Chapter 4.

6.2 Fault Resistance

It is essential to determine maximum fault resistance to calculate minimum fault currents, as different utilities use different values for this purpose. For these values, thresholds for standard overcurrent relay are used as a guide [27]. Therefore, the most remote Line-to-Line fault was simulated at bus 680 of the test system, and the fault resistance was adjusted so that the fault current became twice the total load on the system. This was done because conventional overcurrent relays are often set at about 200% of load current. The maximum fault resistance in this investigation is determined to be 3.8Ω . Beyond this fault resistance, high impedance faults emerged, which are outside the scope of this work. For simulation of bolted faults, minimum fault resistance of $10^{-12} \Omega$ is taken.

6.3 Steady State Simulation

First, the algorithm is tested for the nominal system without fault. The service voltages are observed between $\pm 5\%$ of the nominal voltage for all buses in the system.

6.3.1 Result of Steady State Simulation

As expected, the relay does not pick up for fault during the system's steady state as shown in Table 6.1

Case for	Fault Detected (Yes/No)	Fault Type Identification	Location of Faulted Feeder
Steady State.	No	-	-

Table 6.1: Results for Steady-State Simulation

6.4 Fault Testing and Simulation

This section describes all the configurations of the Test System which is tested for fault simulation. The following configurations are tested and analyzed for the fault simulation summarized in Table 6.2.

1. Single-Source Fault Testing
2. Multi-Source Fault Testing
3. 100 % IBR Penetration

The setup of each configuration is described separately.

All feeder locations are selected to test the relay for a fault on a feeder in each above mentioned configuration. Table 6.2 discriminates all feeder types of the test system into three-phase, two-phase and single-phase. All possible fault types are simulated, including single-line to ground, line-to-line, double-line to ground and three-phase faults depending on the feeder type. The fault resistance varies from minimum to maximum and includes bolted and unbolted faults. Moreover, the distance of fault creation from first bus is taken as 5% , 50% and 95% to test the algorithm for worst case.

The information about the total simulated faults for each configuration of the system is summarized in Table 6.2.

Feeder Type	Faulted Feeder (Bus 1 - Bus 2)	Distance of Fault from Bus 1 (%)	Fault Types	Fault Resistance (Ohm)
Three-phase	Bus 632 - Bus 633	5% , 50% , 95%	ALL possible	10^{-12} to 3.8
Three-phase	Bus 632 - Bus 671	5% , 50% , 95%	ALL possible	10^{-12} to 3.8
Three-phase	Bus 692 - Bus 675	5% , 50% , 95%	ALL possible	10^{-12} to 3.8
Three-phase	Bus 671 - Bus 680	5% , 50% , 95%	ALL possible	10^{-12} to 3.8
Two-phase	Bus 645 - Bus 646	5% , 50% , 95%	ALL possible	10^{-12} to 3.8
Two-phase	Bus 671 - Bus 684	5% , 50% , 95%	ALL possible	10^{-12} to 3.8
Two-phase	Bus 632 - Bus 645	5% , 50% , 95%	ALL possible	10^{-12} to 3.8
Single-phase	Bus 684 - Bus 652	5% , 50% , 95%	ALL possible	10^{-12} to 3.8
Single-phase	Bus 684 - Bus 611	5% , 50% , 95%	ALL possible	10^{-12} to 3.8

Table 6.2: Fault Scenarios for Testing

Note that the feeder from Bus 671 to Bus 692 is not a three-phase line, as it only has an installed breaker for connection/disconnection, so it is not considered part of the analysis.

As seen from Table 6.2, there can be 96 distinct faults for (*four*) three-phase feeders, 54 distinct faults for (*three*) two-phase feeders, and 12 distinct faults for (*two*) single-phase feeders simulated on the Test System. For instance, a single-line to ground bolted fault on the three-phase feeder, Feeder 632-633, created at 5 % distance from the first bus, is considered a single distinct fault. Similarly, other distinct faults on Feeder 632-633 include four possible fault types, three fault distances from the first bus as shown in Table 6.2, and must be analyzed separately for bolted and unbolted fault resistances. This counts as 8 distinct faults on Feeder 632-633 only at a 5 % distance from the first bus. To include all three fault feeder distances, 24 distinct faults are created on Feeder 632-633. Therefore, for (*four*) three-phase feeders in the test system, a total of 96 distinct faults are simulated. The same math is applied to the two-phase and single-phase feeders of the test system.

Finally, this results in a sum of **162 distinct faults** for all feeders of the test system that are simulated and analyzed separately for each configuration described below.

6.4.1 Single Source Fault Testing

In this scenario, only main-grid supplies the distribution system. All the grid-following IBRs are not connected to the system so their status is offline. That is why, this scenario is referred as the single-source fault testing.

As expected, the algorithm detected all faults and correctly identified fault type and faulted feeder location for all 162 distinct faults as shown in Table 6.2 for this configuration.

6.4.2 Multi-Source Fault Testing

In this scenario, the main grid and one or more grid-following IBRs supply the distribution system. That is why this scenario can be referred to as multi-source fault testing in which the microgrid operates in a grid-connected mode.

6.4.2.1 Connection of first IBR

In this scenario, IBR 1 connected to Bus 633 of the system shown in 5.4 is turned ON while the main grid supplies the system. When 0.2 seconds pass after IBR 1 is turned ON, and the system has reached its stable state, the relay is tested for initial fault testing for the modified system. Again,

all possible types of faults are created on six feeder locations of the modified system for both bolted and unbolted faults. This is shown previously in Table 6.2 to maintain a common standard of relay fault testing across the board. The remaining IBRs connected to Bus 680 and 675 are in an OFF state.

As expected, the algorithm detected all faults and correctly identified fault type and faulted feeder location for all 162 distinct faults as shown in Table 6.2 for this configuration.

6.4.2.2 Connection of All IBRs

In this scenario, all three grid-following IBRs connected to Bus 633, Bus 680 and Bus 675 are turned ON while the main grid supplies the system. Each IBR is turned ON individually, one after another, so the distribution system experiences only one transient at a time. After 0.2 seconds is passed following the turning ON of the last connected IBR to the distribution network, the system reaches its stable state and is ready for initial fault testing. Again, all possible types of faults with varying fault resistances are created on six feeder locations as summarized in Table 6.2.

As expected, the algorithm detected all faults and correctly identified fault type and faulted feeder location for all 162 distinct faults as shown in Table 6.2 for this configuration.

6.4.3 100 % IBR Penetration Fault Testing

In this scenario, IBR 1 is turned ON and connected to Bus 650 as a grid-forming inverter to supply the unbalanced currents to balance the system's voltages. Meanwhile, other inverters share the power with a robust droop control to feed the real and reactive loads in the system. This system can also be called the Islanded Mode of microgrid, having 100 % IBR penetration to supply all the loads and losses. The same cases of fault testing as shown in Table 6.2 are applied to the system when it has reached its steady state in the Islanded Mode of operation.

Even in 100 % IBR penetration, the relay detected all 162 distinct faults and correctly identified fault type and faulted feeder location as shown in Table 6.2.

6.4.4 Summary of Results for Fault Testing

The algorithm detected all the faults and correctly identified fault type and faulted feeder location for all the distinct faults as shown in Table 6.2 in all three configurations and cases.

6.5 Dynamic Scenarios Simulation

Besides the faulted scenarios, dynamic scenarios are created to test the security of the relays under non-fault events. The following dynamic scenarios are created during the grid-connected mode of the microgrid.

6.5.1 Load Switching

To simulate the load-switching event, each phase of the unbalanced load on Bus 634 is individually disconnected and reconnected to the system. Besides that, all three phases are simultaneously disconnected and connected back to simulate the load switch ON/OFF events.

The relay did not pick up for the event of load switching as shown in Table 6.3.

Case for	Bus ID	Switched Phases	Fault Detected (Yes/No)	Fault Type Identification	Location of Faulted Feeder
Load Switching	Bus 634	Phase a	No	-	-
Load Switching	Bus 634	Phases a and b	No	-	-
Load Switching	Bus 634	Phases a, b and c	No	-	-

Table 6.3: Results for Load Switching

6.5.2 Capacitor Switching

To induce a capacitor inrush current event, the 600 KVAR capacitor bank at bus 675 was disconnected and reconnected to the system after 0.1 seconds.

The relay did not pick up for the event of capacitor switching as shown in Table 6.4

Case for	Bus ID	Fault Detected (Yes/No)	Fault Type Identification	Location of Faulted Feeder
Capacitor Switching	Bus 675	No	-	-

Table 6.4: Results for Capacitor Switching

6.5.3 Transformer Inrush

To induce a transformer inrush current event, the 500 KVA transformer at bus 633 was disconnected and then connected back to the system after 0.1 seconds. The relay did not pick up

for the event of transformer inrush as shown in 6.5

Case for	Bus ID	Fault Detected (Yes/No)	Fault Type Identification	Location of Faulted Feeder
Transformer Inrush	Bus 633	No	-	-

Table 6.5: Results for Transformer Inrush

6.5.4 Summary of Results for Dynamic Scenarios

For any of the above-explained dynamic scenarios, the relay did not pick up because the first boundary condition for fault detection is not met, which further approves the set voltage threshold described in Chapter 3.

6.6 Summary of Chapter 6

This chapter discusses the simulation and analysis of the Test System shown in Figure 5.4. The modeling of the Test system was done on (EMTP) software - RSCAD. The protection and control logic of the proposed protection scheme was programmed through MATLAB on a PC that acted as a central controller to the system. The phasor values of three-phase LV voltages and currents were obtained and transferred from RSCAD to MATLAB to analyze fault detection, identification, and faulted feeder location based on algorithms discussed in Chapter 4. The phasor values from distributed nodes were synchronized in time. Moreover, all the results described for different cases and scenarios pertain to the offline analysis and simulation of the Test system without accounting for the delay in communicating measurements from RSCAD to MATLAB.

This chapter also determined the maximum and minimum fault resistance to avoid high-impedance faults and included bolted faults for analysis. First of all, the algorithm was tested for the system's steady state. Then, the algorithm was tested for single-source fault testing when all IBRs were offline and only the main grid acted as a source for the distribution system. Besides that, other configurations, including grid-connected mode, were also examined when either one or more IBRs were turned ON in the system for testing. Lastly, the relay was also tested for the configuration of 100% IBR penetration when the main grid was disconnected and all four IBRs involving a grid-forming inverter supplied to the distribution system in islanded mode. For any configuration of the

system, the fault testing of the relay was examined for nine feeder locations, all possible types of fault, and extreme feeder distances, including (5% , 50% and 95%). The relay detected and identified all types of faults and correctly identified faulted feeders for all developed configurations of the Test System. Lastly, the relay did not detect fault for any of the created dynamic scenarios on the Test System, including load switching, capacitor switching and transformer inrush, making it secure and reliable for implementation in distribution systems.

Chapter 7

Conclusions and Discussion

In this study, a (FLISR) protection scheme was developed for renewable-fed distribution systems using Low-voltage (LV) sensors. First, an overview of the cost-effective and commercially available sensors and (IEDs) that can assist in the actual implementation of the scheme was provided to support the feasibility of the LV sensors assumed for this work. The protection scheme was developed by developing network equations based on the measurements made at the LV side of each customer transformer. The rationale developed to detect a fault, fault type and faulted feeder was developed in a way that is independent of network topology, IBR location, or connection status. This methodology was codified into a relay algorithm.

For the validation of proposed protection scheme, a test system based on IEEE 13 Bus Feeder was adopted. The modeling of the test system was done on Electromagnetic Transient (EMT) platform in real time using RSCAD. This platform helped speed up the simulations with IBRs. The protection logic of proposed protection scheme was programmed through MATLAB on a PC that acted as a central controller to the system. The test system was simulated for both grid-connected and stand-alone modes of (MG) having 100 % IBR penetration in the islanded mode. The controller successfully detected and identified the type of fault and located the correct faulted feeder for all simulated faults on the test system. Besides that, the test system was also examined under the simulation of dynamic scenarios, including transformer inrush, load switching, and capacitor switching. The controller did not identify any of the dynamics as faults, which further complements the security of the proposed protection scheme.

7.1 Further Research

This study did not account for communication delay for the transfer of synchronized LV measurements to the central controller, which will depend on the communication platform designed for the microgrid controller. This can be targeted for future work. With this in place, the relay can be tested in real time using co-simulation of the physical and cyber layers, with controller as hardware in the loop (HIL).

Additionally, the ‘location of fault’ in the proposed protection scheme accounts for identifying faulted feeder in the system. In this regard, the additional scope of work consists of computing the exact location of fault on the faulted feeder. The fault location scheme described in [32] can be used for this purpose and implementation in real time.

Future work will also include testing the proposed protection scheme on a more extensive test system, including a mesh distribution network and feeder reconfiguration.

Appendices

Appendix A KCL Expressions for the Test System

The following section includes the expressions of KCL written for each and every bus of the system as shown in Figure 5.4. These expressions are integral part of the algorithm of faulted feeder identification and are utilized for the programming of central controller in validation of proposed protection scheme.

$$KCL_{\text{Bus632}} = I_{\text{Line650632}} - I_{\text{Load632}} - I_{\text{Line632633}} - I_{\text{Line632671a}} - I_{\text{Line632645}} \quad (1)$$

$$KCL_{\text{Bus633}} = I_{\text{Line632633}} + I_{\text{inv2}} - I_{\text{Load633}} \quad (2)$$

$$KCL_{\text{Bus671a}} = I_{\text{Line632671a}} - I_{\text{Load671a}} - I_{\text{Line671a671}} \quad (3)$$

$$KCL_{\text{Bus671}} = I_{\text{Line671a671}} - I_{\text{Load671}} - I_{\text{Line671680}} - I_{\text{Line671692}} - I_{\text{Line671684}} - I_{\text{Load692}} \quad (4)$$

$$KCL_{\text{Bus675}} = I_{\text{Line692675}} + I_{\text{inv3}} - I_{\text{Load675}} \quad (5)$$

$$KCL_{\text{Bus680}} = I_{\text{Line671680}} + I_{\text{inv4}} - I_{\text{Load680}} \quad (6)$$

$$KCL_{\text{Bus645}} = I_{\text{Line632645}} - I_{\text{Load645}} - I_{\text{Line645646}} \quad (7)$$

$$KCL_{\text{Bus646}} = I_{\text{Line645646}} - I_{\text{Load646}} \quad (8)$$

$$KCL_{\text{Bus684}} = I_{\text{Line671684}} - I_{\text{Load684}} - I_{\text{Line684652}} - I_{\text{Line684611}} \quad (9)$$

$$KCL_{\text{Bus652}} = I_{\text{Line684652}} - I_{\text{Load652}} \quad (10)$$

$$KCL_{\text{Bus611}} = I_{\text{Line684611}} - I_{\text{Load611}} \quad (11)$$

$$KCL_{\text{Bus692}} = I_{\text{Line671692}} - I_{\text{Load692}} - I_{\text{Line692675}} \quad (12)$$

Here, the terminology for representing KCL at a given bus, line currents and load currents represents the terminology described in Section 1.4 of Chapter 2. For instance, KCL at Bus 633 is computed from Equation 2 where each element of the expressions represents the following:

KCL_{Bus633} represents the (3x1) matrix of the KCL computed at Bus 633.

$I_{\text{Line632633}}$ represents the (3x1) matrix of three-phase current phasors calculated for the line between Bus 632 and Bus 633.

I_{Load633} represents the (3x1) matrix of three-phase current phasors calculated on the primary side of the Transformer connected to Bus 633, rated at 2401 V for each phase.

I_{inv2} represents the (3x1) matrix of three-phase current phasors calculated to show the currents supplied to Bus 633 by inverter 2, rated at 2401 V for each phase.

That is how the terminology for other buses remains the same. See the above example for the terminology of the representation of KCL at Bus 633. This includes a (3x1) matrix of phasors three-phase line currents, load currents and inverter currents, all of which are calculated and rated at 2401 V for each phase.

Bibliography

- [1] M. J. Reno, S. Brahma, A. Bidram, and M. E. Ropp, “Influence of inverter-based resources on microgrid protection: Part 1: Microgrids in radial distribution systems,” *IEEE Power and Energy Magazine*, vol. 19, no. 3, pp. 36–46, 2021.
- [2] P. Gadde and S. M. Brahma, “Topology-agnostic, scalable, self-healing, and cost-aware protection of microgrids,” *IEEE Transactions on Power Delivery*, vol. 37, no. 4, pp. 3391–3400, 2021.
- [3] A. Zamani, A. Rajapakse, B. Kazimier, B. Mackie, E. Song, J. Deaton, J. Niemira, J.-N. Paquin, J. Burnworth, J. O’Brien, *et al.*, “Microgrid protection systems,” tech. rep., Technical Report PES-TR71, 2019.
- [4] W. Ajaz and D. Bernell, “Microgrids and the transition toward decentralized energy systems in the united states: A multi-level perspective,” *Energy Policy*, vol. 149, p. 112094, 2021.
- [5] T. Patel, P. Gadde, S. Brahma, J. Hernandez-Alvidrez, and M. J. Reno, “Real-time microgrid test bed for protection and resiliency studies,” in *2020 52nd North American Power Symposium (NAPS)*, pp. 1–6, IEEE, 2021.
- [6] G. Kaur, A. Prakash, and K. U. Rao, “A critical review of microgrid adaptive protection techniques with distributed generation,” *Renewable Energy Focus*, vol. 39, pp. 99–109, 2021.
- [7] ABB, “Fault passage indicator product guide on remote i/o unit rio600.” Available: <https://new.abb.com/medium-voltage/digital-substations/protection-relays/remote-i-o/remote-io-unit-rio600/>. [Online; Accessed 5-June-2024].
- [8] Eaton, “Technical catalog on current and voltage sensors.” Available: <https://www.eaton.com/content/dam/eaton/products/industrialcontrols-drives-automation-sensors/current-and-voltage-sensors-v8-t7-ca08100010e.pdf>. [Online; Accessed 3-June-2024].
- [9] ABB, “Catalog for distribusense sensors enhancing grid reliability and efficiency.” Available: https://library.e.abb.com/public/01592695299041489e3db6a1230fcfbf/1VAP420011-DB_DistribuSense%20overview_111721.pdf. [Online; Accessed 4-June-2024].
- [10] National Control Devices, “Product on dual 120vac mains voltage monitor with iot interface.” Available: <https://store.ncd.io/product/dual-120vac-mains-voltage-monitor-with-iot-interface/>. [Online; Accessed 5-June-2024].
- [11] ABB, “Technical guide and catalog on current and voltage sensors.” Available: <https://acrobat.adobe.com/link/review?uri=urn%3Aaaid%3Ascds%3AUS%3A98f98218-fb71-33f2-bcbf-8ef140df2a98>, 2015. [Online; Accessed 5-June-2024].
- [12] A. Swain, E. Abdellatif, A. Mousa, and P. W. Pong, “Sensor technologies for transmission and distribution systems: A review of the latest developments,” *Energies*, vol. 15, no. 19, p. 7339, 2022.

- [13] V. C. Gungor, B. Lu, and G. P. Hancke, "Opportunities and challenges of wireless sensor networks in smart grid," *IEEE Transactions on Industrial Electronics*, vol. 57, no. 10, pp. 3557–3564, 2010.
- [14] M. Nordman *et al.*, *An architecture for wireless sensors in distributed management of electrical distribution systems*. Helsinki University of Technology, 2004.
- [15] R. Moghe, F. C. Lambert, and D. Divan, "Smart "stick-on" sensors for the smart grid," *IEEE Transactions on Smart Grid*, vol. 3, no. 1, pp. 241–252, 2012.
- [16] F. Zavoda, C. Abbey, Y. Brissette, and R. Lemire, "Universal ied for distribution smart grids," in *22nd International Conference and Exhibition on Electricity Distribution (CIRED 2013)*, pp. 1–4, 2013.
- [17] E. Bjerkan, "Efficient fault management using remote fault indicators," in *CIRED 2009-20th International Conference and Exhibition on Electricity Distribution-Part 1*, pp. 1–4, IET, 2009.
- [18] E. Dusabimana and S.-G. Yoon, "A survey on the micro-phasor measurement unit in distribution networks," *Electronics*, vol. 9, no. 2, p. 305, 2020.
- [19] North American Synchrophasor Initiative (NASPI), "Reference document for micro-pmu installation." Available: https://www.naspi.org/sites/default/files/reference_documents/uPMU%20Installation%20Ref%20Manual%20Mar%2023%202018.pdf, 2018. [Online; Accessed 26-June-2024].
- [20] Powerside, "micropmu synchrophasors." Available: <https://powerside.com/products/power-quality-measurement-solutions/micropmu-synchrophasor/>, 2022. [Online; Accessed 26-June-2024].
- [21] Power Sensors Limited, "Synchrophasors for distribution, microgrids:." Available: http://www.pqs.it/Download/MicroPMU_Data_Sheet_Rev1_3ITA.pdf. [Online; Accessed 26-June-2024].
- [22] S. Chakraborty, S. Das, T. Sidhu, and A. Siva, "Smart meters for enhancing protection and monitoring functions in emerging distribution systems," *International Journal of Electrical Power & Energy Systems*, vol. 127, p. 106626, 2021.
- [23] Powerside, "Power analyzers: Uncover hidden power quality problems." Available: <https://powerside.com/products/power-quality-measurement-solutions/pqube-3-power-analyzers/>, 2022. [Online; Accessed 26-June-2024].
- [24] Quanta Technology, "Report on distribution synchronized measurements roadmap." Available: https://www.naspi.org/sites/default/files/reference_documents/distribution_synch_measurement_roadmap_20210927.pdf, 2021. [Online; Accessed 10-June-2024].
- [25] K. P. Schneider, B. A. Mather, B. C. Pal, C.-W. Ten, G. J. Shirek, H. Zhu, J. C. Fuller, J. L. R. Pereira, L. F. Ochoa, L. R. de Araujo, R. C. Dugan, S. Matthias, S. Paudyal, T. E. McDermott, and W. Kersting, "Analytic considerations and design basis for the ieeec distribution test feeders," *IEEE Transactions on Power Systems*, vol. 33, no. 3, pp. 3181–3188, 2018.
- [26] S. M. Brahma, P. L. De Leon, and R. G. Kavasseri, "Investigating the option of removing the antialiasing filter from digital relays," *IEEE Transactions on Power Delivery*, vol. 24, no. 4, pp. 1864–1868, 2009.
- [27] A. Gujar and S. Brahma, "Comparison of legacy relay with machine learning based relay for detecting faults at inverter terminals in a distribution system with inverter based resources," in *2023 North American Power Symposium (NAPS)*, pp. 1–6, IEEE, 2023.

- [28] W. H. Kersting, "Distribution system modeling and analysis," in *Electric power generation, transmission, and distribution*, pp. 26–1, CRC press, 2018.
- [29] D. G. Photovoltaics and E. Storage, "Ieee standard for interconnection and interoperability of distributed energy resources with associated electric power systems interfaces," *IEEE std*, vol. 1547, pp. 1547–2018, 2018.
- [30] P. H. Gadde and S. Brahma, "Realistic microgrid test bed for protection and resiliency studies," in *2019 North American Power Symposium (NAPS)*, pp. 1–6, 2019.
- [31] ABB, "Low voltage dry type transformers percent impedance." Available: <https://library.e.abb.com/public/eb4bfdafc6954a3387b2c2d6e6e6535f/LVDTT%20percent%20impedance%2020230725-1.pdf?x-sign=ZC3e5Vbr15+Iw9vsQ5T3AUezf9m+8Mp0QUav+xtezIt635Wecj0wqjZ0Bm7ASZPx>, 2023. [Online; Accessed 5-June-2024].
- [32] A. A. Girgis, D. G. Hart, and W. L. Peterson, "A new fault location technique for two-and three-terminal lines," *IEEE Transactions on Power Delivery*, vol. 7, no. 1, pp. 98–107, 1992.